Supplementary Figures and Tables

This PDF file includes:

Supplementary Methods
Figs. S1 to S19
Tables S1 to S6
Captions for Movies S1 to S2

Other Supplementary Materials for this manuscript include the following:

Table S7

Movies S1 to S2

Supplementary Methods

Preclinical studies in mice

Animals. All mice (494 males and 150 females) were housed under specific pathogen-free conditions in a temperature-controlled room (21-22°C) with a 12h light/dark cycle. The day the litters were born was considered postnatal day 0 (P0). Animals were weaned at P21 and were provided with *ad libitum* access to chow diet (Scientific Diets, SAFE A03) and water.

Ts65Dn *(B6EiC3Sn.BliA-Ts(1716)65Dn/DnJ; Stock no. 005252*) mice (*24, 83, 84*) carrying a partial trisomy of chromosome 16, the orthologous region of human chromosome 21, were purchased from Jackson Laboratories (New Harbor, ME, USA). As the Ts65Dn line has a genetic background wild-type (WT) for the Pde6b gene, the line was maintained by crossing Ts65Dn trisomic females with Pde6b+ males (C57BL/6JeiJ x C3Sn.BliA-Pde6b+/DnJ)F1/J; Stock no 003647). This mating system produced Ts65Dn animals and WT littermates used in this study. *Gnrh::Cre* (Tg(Gnrh1::Cre)1Dlc), *Dicer*$^{loxP/loxP}$, and *Gnrh::Gfp* mice were a generous gift from Dr. Catherine Dulac (Howard Hughes Medical Institute, Cambridge MA) (*85*), Dr. Brian Harfe (University of Florida, FL) (*86*) and Dr. Daniel J. Spergel (Section of Endocrinology, Department of Medicine, University of Chicago, IL) (*87*), respectively. Importantly, only male *Gnrh::Cre* mice are used to generate bigenic mice (i.e., crossed with *BoNTB*$^{loxP\text{-}STOP\text{-}loxP}$ or Ts65Dn female mice), since recombination in this mouse line can occur in some oocytes (*88*). Tg(CAG-BoNT/B,EGFP)U75-56wp/J (*BoNTB*$^{loxP\text{-}STOP\text{-}loxP}$) mice and *GnRHR::Cre*;*Tau-Gfp*$^{LoxP\text{-}STOP\text{-}LoxP}$ mice were generated as described before (*89, 90*). *THY*::*TAU22* male mice, which express human 4-repeat tau mutated at sites G272V and P301S under a Thy1.2-promotor and that display tau pathology in the absence of any motor dysfunction (*66*), entered the experimental procedure at 12-month-old. Mice were genotyped by PCR using the primers listed in **Table S3.**

Animal studies were approved by the Institutional Ethics Committee for the Care and Use of Experimental Animals of the University of Lille (APAFIS# 29172-2020121811279767 v5) and the University of Lyon 1 (APAFIS#10164-2017060710541958 v4), and all experiments were performed in accordance with the guidelines for animal use specified by the European Union Council Directive of September 22, 2010 (2010/63/EU). The sex of the animals used is specified in the text and/or figure legends. Observers were blind to the genotype or/and treatment group of animals in the study except when the morphological or physiological differences were too obvious to be ignored.

Drugs. Clozapine N-oxide hydrochloride (SML2304, Sigma) was dissolved in sterile saline (0.9% NaCl) and stored at 4°C. On the day of injection, the CNO stock was brought to room temperature and diluted in sterile saline (0.9% NaCl). Lutrelef (Ferring Pharmaceuticals, Switzerland) was dissolved in sterile 0.1M PBS and stored at 4°C. The day before osmotic minipumps and programmable micro-infusion pumps were implanted, the Lutrelef stock was brought to room temperature and diluted in sterile 0.1M PBS. GnRH-1 peptide (Genecust) was dissolved in sterile water, aliquoted and stored at -80°C. On the day of injection, the GnRH-1 stock was thawed and diluted in a solution of sterile saline.

Physiological measurements. *Puberty and cyclicity*. Males were checked for balanopreputial separation and urine samples were collected daily from weaning to P45. Weaned female mice were checked daily for vaginal opening. After vaginal opening, vaginal smears were performed daily and analyzed under an inverted microscope to identify the phase of the estrous cycle. *Fertility index*. Female fertility indices were calculated from the number of litters per female during a 120-day-long mating period.

Pulsatile LH measurements. Adult mice were habituated by daily handling. Blood samples (5 µL) were taken from the tip of the tail at 10 min intervals over a period of 2 h (between 10:00 and 12:00), diluted in 45 µL of 1X PBS-T (0.05%) and immediately frozen and stored at -80°C. LH levels were determined using a sensitive LH sandwich ELISA that has been previously described (*91*). Pulses were confirmed using DynPeak (*92*).

Urine collection and protein analysis. To assess major urinary protein (MUP) profile diversity, urine was collected from weaning to P45 in male mice following either spontaneous urination when handled, or provoked by exerting a gentle pressure on the mouse bladder. The urine was collected in microcentrifuge tubes kept on ice during the collection procedure. All samples were initially frozen at –20°C then kept at –80°C until further processing. For protein analysis by western blotting (WB), 1 µl of urine was mixed with 1X sample buffer (Invitrogen) and 1X reducing agent (Invitrogen). Samples were boiled for 5 min and electrophoresed for 75 min at 150 V on 4–12% MES SDS-polyacrylamide gels according to the protocol supplied with the NuPAGE system (Invitrogen). After migration, the proteins were transferred onto a 0.2 µm nitrocellulose membrane (Invitrogen) using the blot module of the NuPAGE system (Invitrogen) for 90 min at 30V on ice. Membranes were then blocked for 1 h in blocking buffer [TBS with 0.05% Tween 20 (TBST) and 5% non-fat dry milk] at room temperature, and incubated for 48 h at 4°C with the

primary antibody (rabbit polyclonal anti-MUP1, 1:200 dilution, sc-66976, Santa Cruz Biotechnology, Inc, RRID:AB 1126410) diluted in blocking buffer. Following this, membranes were washed three times with 1X TBST before incubation with the secondary antibody (peroxidase-conjugated anti-rabbit IgG (H+L), 1:2000 dilution, PI-1000, Vector Laboratories, RRID:AB 2916034) diluted in blocking buffer for 1 h at room temperature. After incubation with secondary antibody, the membranes were washed three times with 1X TBST. Immunoreactions were developed using the ECL detection kit (NEL101; PerkinElmer, Boston, MA) and scanned using a desktop scanner (Epson Expression 1680 PRO).

Brain tissue dissection. Mice were euthanized by decapitation. The hippocampus, cortex and preoptic area (POA) of the hypothalamus were dissected using Wecker scissors (Moria, France) under a binocular magnifying glass, placed in dry ice immediately and stored at – 80°C until further processing and assays.

Tissue protein extraction and WB analyses. *Expression of Alzheimer-related proteins*. Both hippocampus and cortex from adult Ts65Dn and WT mice were sonicated in 400 µL (for hippocampus) or 800 µL (for cortex) of lysis buffer (10 mM Tris pH 7.4, 10% sucrose and proteases inhibitors (1 pellet for 10mL Complete; Roche Diagnostics GmbH) and stored at –80°C until use. Protein concentration was determined using the BCA assay (Pierce), subsequently diluted with 2X LDS (Life) and supplemented with reducing agent (Life). Samples were boiled for 10min at 100°C. Proteins were separated on precast 12% Criterion XT Bis-Tris polyacrylamide gels (Bio-Rad) using 1X MOPS SDS running buffer. Subsequently, proteins were transferred onto a 0.4 µm nitrocellulose membrane (G&E Healthcare). For low molecular weight proteins, such as carboxy-terminal fragments of APP (CTFs), 16.5% Criterion XT Tris-Tricine polyacrylamide gels (Bio- Rad) and 1X Tris-Tricine SDS running buffer were used. Proteins were transferred onto a 0.2 µm nitrocellulose membrane (G&E Healthcare). For estimation of molecular weights, a molecular weight marker (Novex and Magic Marks, Life Technologies) was simultaneously run. Membranes were incubated in blocking buffer [TNT (Tris 15 mM pH 8, NaCl 140 mM, 0.05% Tween) and 5% non-fat dry milk or 5% bovine serum albumin (BSA)] at RT and incubated overnight at 4°C with the appropriate primary antibody (**Table S5**) diluted in blocking buffer (TNT with 5% milk or BSA). Following this, membranes were incubated with the corresponding secondary antibodies (**Table S5**). Immunoreactions were developed using chemiluminescence kits (ECL™, Amersham Bioscience) and visualized using a LAS3000 imaging system (Fujifilm).

Results were normalized to GAPDH and quantification was performed using ImageJ software (Scion Software).

Expression of miR-200b^{POA}-regulated proteins in the hippocampus. Hippocampal samples were microdissected from the brain of the models described above. Samples were kept at -80 degrees until their use. Hippocampus protein were extracted with 150µl of freshly prepared lysis buffer [25mM Tris pH 7.4, 50 mM β-glycerophosphate, 1% Triton x100, 1.5 mM EGTA, 0.5mM EDTA, 1 mM sodium orthovanadate, 10 µg/ml Leupeptin and Pepstatin A, 10 µg/ml aprotinin, 100 µg/ml PMSF (reagents sourced from Sigma Aldrich, St. Louis MO, USA)]. Protein extracts were then homogenized using a 26 gauge needle before centrifugation at 12,000g for 15 mins at 4°C. The supernatant was recovered and protein quantified using the Bradford method (BioRad, Hercules, CA). 1x sample and 1x loading buffer (ThermoFisher, Invitrogen) was added to the samples, which were then boiled for 5 min before electrophoresis at 120V for 100 mins in 5–12% tris-acetate precast SDS-polyacrylamide gels according to the protocol supplied with the NuPAGE system (ThermoFisher, Invitrogen). After size fractionation, the proteins were transferred onto a PVDF membrane (0.2µm pore size, LC2002; Invitrogen, Carlsbad CA, USA) in the blot module of the NuPAGE system (ThermoFisher, Invitrogen) maintained at 1A for 75 min at room temperature (RT). Blots were blocked for 1h in tris-buffered saline with 0.05% Tween 20 (TBST) and 5% non-fat milk at RT, incubated overnight at 4°C with their respective primary antibody in TBST 5% bovine serum albumin (Sigma Aldrich, Cat A7906), and washed four times with TBST before being exposed to horseradish peroxidase-conjugated secondary antibodies diluted in 5% non-fat milk TBST for 1h at RT. The immunoreactions were detected with enhanced chemiluminescence (NEL101; PerkinElmer, Boston, MA).

Orchidectomy. Adult males were subjected to bilateral gonadectomy under isoflurane anesthesia through a small ventral midline incision in the scrotum, which was subsequently sealed.

Behavioral studies.

Homing test. For 30 min at the beginning of the light period, 9-day old pups were separated from the dam and kept at a temperature of 35 ◦ C in a holding cage. Individual pups were then transferred to a Plexiglas cage (391 × 199 mm, walls 160 mm high) containing bedding from the home cage evenly distributed on one side (140 × 199 mm, "goal area") and the rest of the cage covered with clean wood shavings (“start area”). Each pup was placed close to the wall on the opposite side. The time taken by the pup to place both forelimbs above the goal area was recorded (cutout time

240 s) (*93*). In addition, the pup's spontaneous motor activity was measured using EthoVision video tracking equipment and software (Noldus Bv, Wageningen, The Netherlands).

Habituation/dishabituation test. The habituation/dishabituation test was used to assess the ability to differentiate between different odors (*28*). Mice were housed singly for 8 days prior to testing. This olfactory test included a presentation of acetophenone (00790, Sigma) for habituation and octanal (05608, Sigma) for dishabituation, or vice versa. Before the test, mice were allowed to explore the open-field area and an empty odor box for 30 min. After this habituation period, mice were presented with a first odor for four consecutive trials of a duration of 1 min each, with an inter-trial interval of 10 min to ensure the clearing of the odor. After these four consecutive trials, a second odor was presented during a 1 min trial. Odors (20µl of a 1:1000 stock dilution) were presented on a filter paper placed in a perforated plastic box to avoid allowing the mice to be in direct contact with them. The total amount of time the mouse spent sniffing the object during different trials was recorded and quantified. The habituation/dishabituation test was performed at the beginning of the light period (9:00) and on the day of diestrus1 in females.

Novel object recognition test. Recognition memory was assessed using the novel object recognition test (*94*). Mice were housed singly for 5 days prior to testing. On day 1, two identical objects (A+A) were placed within the open-field arena on opposite sides of the cage, equidistant from the cage walls. Each mouse was placed between the two objects and allowed to explore them for 15 min. Day 2 consisted of two phases, a familiarization and a test phase. During the familiarization phase (trial 1), which lasted 15 min, the mice explored two other identical objects (B+B). After this phase, the mice were replaced in their home cage for 1 hour before starting the test phase. During the test phase, one object from trial 1 and a completely new object (B+C) were placed within the open-field area and mice were allowed to explore them for 5 min (trial 2). The object recognition score was calculated as the time spent exploring the new object (trial 2) over the total exploration time, and was used to evaluate recognition memory. The object recognition test was performed at the beginning of the afternoon (14:00) and initiated on the day of diestrus1 (day1) in females.

Y-maze test. Natural spontaneous exploratory behavior and visuospatial short-term memory were tested using the Y-maze (*95, 96*). The Y-maze consists of three white wooden arms (24.0 cm x 6.5 cm x 15 cm), elevated to a height of 41.0 cm above the floor and surrounded with visual cues on the wall. Mice were placed in the start arm, facing the end of this arm, and were allowed to explore

the maze for 10 min while one arm was blocked (novel arm). Consequently, mice were placed in their home cage for 1 h before being allowed to explore all three arms for 5 min. The trajectories of the mice were recorded using EthoVision video tracking equipment and software (Noldus Bv, Wageningen, The Netherlands). The time spent in the novel arm and latency to enter the novel arm were compared between mice. The Y-maze test was performed at the beginning of the afternoon (14:00).

Electrophysiological studies. Male WT, Ts65Dn and Ts65Dn+miR200b mice aged 5-7 months were studied. The animals were housed under standard laboratory conditions; 12:12 h light-dark cycle with free access to food and water.

The amplitude of population spikes and field excitatory post-synaptic potentials (fEPSPs) from CA1 stratum radiatum of the right hippocampal hemisphere was recorded in chloral hydrate-anesthesia (3.5%, i.p.) mouse placed in a stereotaxic frame (Sakata et al., 2000), and maintained at a constant body temperature of 37 °C. Unilateral implantations of electrodes were performed using standard stereotaxic procedures. Briefly, a bipolar stimulating electrode (NEX-200, Rhodes Medical Instruments, USA was lowered to the left side of the hippocampal commissural fibers (-1.8 mm. from bregma, 1.5 mm. from the midline, 1.3 to 1.4 mm. from the surface of the cortex) and a recording single-barreled glass micropipette (tip broken back to 2 to 4 μm and filled with a 2 M NaCl solution saturated with blue Chicago dye) was positioned in the right CA1 area of the hippocampus (-2.5 mm from bregma, 2.3 mm. from the midline, 1.2 to 1.3 mm. from the surface of the cortex). The final depths of the stimulating and the recording electrodes were determined by optimizing the amplitude of the population spike and fEPSPs in the CA1 area. The position of the stimulating electrode was the same for both population spike and fEPSPs recordings. Electrode positions were optimized to record maximal field responses evoked at a frequency of 0.033 Hz following electrophysiological criteria (Leung, 1979): (i) the amplitude of evoked potential depends on stimulation intensity (input–output curves from 200 to 1000 μA), and (ii) a facilitation of the second pulse occurred when we applied a paired pulse with an interval inter stimulation of 30 to 1000 ms. At the beginning of each experiment, input–output and paired-pulse stimulation curves were obtained first with population spike response followed by that of fEPSP.

RNA isolation from POA and quantitative RT-PCR analyses. Total RNA, containing mRNA and microRNA, was extracted using the Ambion mirVana™ microRNA Isolation Kit (Ambion, Inc;

CA, USA) from POA fragments triturated by passing them through 22 and 26 gauge needles in succession. The quality and concentration of RNA were determined by spectrophotometry using an ND-1000 NANODROP 385 (Thermo-scientific). For gene expression analyses, mRNAs were reverse transcribed using SuperScript® III Reverse Transcriptase (Life Technologies). Real-time PCR was carried out on an Applied Biosystems 7900HT Fast Real-Time PCR System using exon-boundary-specific TaqMan® Gene Expression Assays (Applied Biosystems) (**Table S6**). For Mbp, Kcnj13, Id4 and Aqp1 expression analysis, cDNA was synthetized from 300ng of total RNA using the Maxima First Strand cDNA Synthesis Kit (Thermo Scientific) under manufacturer's recommended conditions. Real-time PCR was carried out on the T100 Thermal cycler (Bio-Rad) using the PowerUP SYBR Green Master Mix (Applied Biosystems), data were analyzed using the 2-ΔΔCT method (*97*) and normalized to both Polr2a and 36b4 housekeeping gene levels.

MicroRNA expression analyses were performed using specific TaqMan RT primers and the TaqMan miRNA Reverse Transcription Kit (Applied Biosystems), followed by quantitative real-time PCR using predesigned assays for microRNAs (Applied Biosystems) (**Table S6**) on an Applied Biosystems 7900HT thermocycler using the manufacturer's recommended cycling conditions. Gene and miRNA expression data were analyzed using SDS 2.4.1 and Data Assist 3.0.1 software (Applied Biosystems).

Isolation of hypothalamic GnRH neurons and quantitative RT-PCR analyses. The POA of *Gnrh::Gfp* and *Gnrh::Gfp;Ts65Dn* mice were microdissected and enzymatically dissociated using a Papain Dissociation System (Worthington, Lakewood, NJ) to obtain single-cell suspensions. Fluorescence-activated cell sorting (FACS) was performed using a FACS ARIA SORP apparatus (BD Bioscience). Sorting was based on measurements of GFP fluorescence (excitation: 488nm, 50 mW; detection: GFP bandpass 530/30 nm, autofluorescence bandpass 695/40nm) (**Fig. S6**). For each animal, GFP-positive and -negative cells were sorted directly into 10 µl extraction buffer [0.1% Triton® X-100 (Sigma-Aldrich) and 0.4 U/µl RNaseOUT™ (Life Technologies)].

In order to analyze gene expression, mRNAs obtained from FACS-sorted GnRH neurons were reverse transcribed using SuperScript® III Reverse Transcriptase (Life Technologies) and a linear pre-amplification step was performed using the TaqMan® PreAmp Master Mix Kit protocol (P/N 4366128, Applied Biosystems). Real-time PCR was carried out on an Applied Biosystems 7900HT Fast Real-Time PCR System as described previously, using specific TaqMan® Gene Expression Assays (Applied Biosystems) (**Table S6**).

Preparation of donor tissues and neuronal grafting. Donor tissue for the POA grafts were obtained from postnatal day 2 (P2) WT mice, containing GnRH neurons capable of releasing GnRH (WT-POA), and *Gnrh::Cre*; *BoNTB*$^{loxP\text{-}STOP\text{-}loxP}$ mice, containing GnRH neurons incapable of release (*BoNTB*^{Gnrh}-POA). The tissues were microdissected and enzymatically dissociated using a Papain Dissociation System (Worthington, Lakewood, NJ) to obtain a cell suspension in 5 µl 1X HBSS solution. Two POAs were used per implant. Adult Ts65Dn mice were placed in a stereotaxic frame (Kopf® Instruments, California) under anesthesia (isoflurane), and a burr hole was drilled -1.7 mm from Bregma at the midline, according to a mouse brain atlas (*98*). A 25 µl Hamilton syringe (22-gauge needle) was slowly inserted into the 3v (5.6 mm deep relative to the dura), and 5 µl of either WT-POA or *BoNTB*^{Gnrh}-POA cell suspension were injected using an infusion pump (KD Scientific, Holliston, MA) over 10 min. Under the same conditions, control adult Ts65dn and WT mice were injected with 5µl of vehicle solution (HBSS 1X) (sham groups).

Viruses and stereotaxic injections. Mice were anaesthetized (1% isoflurane in 0.7 l/min airflow) and placed on a stereotaxic frame (Kopf® Instruments, California). The injection was carried out using a 2 µl 25 gauge Hamilton syringe at a rate of ~40 nl/min, and the needle was kept in place for 5 min before and 7 min after the injection. Injection coordinates were based on the Paxinos mouse brain atlas (*98*). To target hypophysiotropic GnRH neurons adult *Gnrh::Cre* mice received a unilateral injection of AAV-eYFP (AAV9.EF1a.DIO.eYFP.WPRE.hGH, 1×10^{13} vg/ml; Addgene plasmid # 27056, RRID:Addgene_27056) into the ME (anteroposterior (AP):-1.7 mm, medio-lateral (ML):-0.2 mm, dorsoventral (DV): –6.1 mm) with 300 nl at a rate of 50 nl per minute.

Cre-dependent Designer Receptors Exclusively Activated by Designer Drugs (DREADDs) were used to study the effect of GnRH neuronal activation. The plasmid pAAV-EF1a-DIO-hM3D(Gq)-mCherry was a gift from Bryan Roth (Addgene plasmid # 50460, RRID:Addgene_50460) and viral preparation was carried out at the Molecular Biotechnology Centre (MBC; Prof. Emilia Turco Lab), University of Turin, Italy. The viral construct AAV9.EF1a.DIO.hM3D(Gq)-mCherry was injected bilaterally (250 nl or 500 nl total; 2×10^{13} gc/ml) into the rPOA (AP:+0.8 mm, ML:±0.1 mm, DV: –5.1 mm) of adult *Gnrh*::*cre* and Ts65Dn; *Gnrh*::*cre* mice.

To selectively overexpress the miR-200 family, particularly miR-200b, adult Ts65Dn mice received a unilateral injection with scAAV9-EF1a-mmu-miR-200b-eGFP (AAV-miR200b, 2.1×10^{13} gc/ml) or scAAV9-EF1a-ctrl-miR-eGFP (AAV-GFP, 2.2×10^{13} gc/ml, RRID:Addgene_44362) (Vector Biolabs) into the rPOA. We used a 300-nl total volume injecting

the virus in two steps along the DV coordinate of DV: -5.3 and –5.1 mm with 150 nl at each point, and both points at AP = + 0.8 mm and ML = 0.

To selectively inhibit the activity of hippocampal neurons expressing the GnRH receptor, we used a Cre-dependent inhibitory DREAADs approach in *Gnrhr*::*cre* mice. The AAV8-hSyn-DIO-hM4D-mCherry (Prep# UPV-920; 250 nl or 500 nl total; 1.1×10^{13} gc/ml) was stereotactically infused bilaterally into the hippocampus (AP: -2.06, ML: ±1.8; DV: -1.3).

RNA-sequencing. Total RNA was isolated from frozen POA and hippocampus using the RNeasy Lipid Tissue Mini Kit (Qiagen; Cat # 74804) following the manufacturer's instructions. Samples exhibited RNA Integrity Number (RIN) ≥ 9. RNA-Seq libraries were generated from 500 ng of total RNA using TruSeq Stranded mRNA Library Prep Kit and TruSeq RNA Single Indexes kits A and B (Illumina, San Diego, CA), according to manufacturer's instructions. Briefly, following purification with poly-T oligo attached magnetic beads, the mRNA was fragmented using divalent cations at 94C for 2 minutes. The cleaved RNA fragments were copied into first strand cDNA using reverse transcriptase and random primers. Strand specificity was achieved by replacing dTTP with dUTP during second strand cDNA synthesis using DNA Polymerase I and RNase H. Following addition of a single 'A' base and subsequent ligation of the adapter on double stranded cDNA fragments, the products were purified and enriched with PCR (30 sec at 98C; [10 sec at 98C, 30 sec at 60C, 30 sec at 72C] x 12 cycles; 5 min at 72C) to create the cDNA library. Surplus PCR primers were further removed by purification using AMPure XP beads (Beckman-Coulter, Villepinte, France) and the final cDNA libraries were checked for quality and quantified using capillary electrophoresis. Libraries were then single-read sequenced with a length of 50 pb, with 8 samples per lane on an Illumina Hiseq4000 sequencer. Image analysis and base calling were carried out using RTA v.2.7.3 and bcl2fastq v.2.17.1.14. Reads were mapped onto the mm10 assembly of Mus musculus genome using STAR (*99*) v.2.5.3a. Gene expression was quantified from uniquely aligned reads using HTSeq-count (*100*) v.0.6.1p1 with annotations from Ensembl release and union mode. Data quality was evaluated with RSeQC (*101*). Comparisons of read counts were performed using R 3.5.1 with DESeq2 (*102*) v1.22.1 Bioconductor package. More precisely, counts were normalized from the estimated size factors using the median ratio method and a Wald test was used for the statistical test. Un-wanted variation was identified with SVA (*103*) and considered in the statistical model. To reduce false positive, p-values were adjusted by IHW method (*104*). In total, 4 biological replicates were used per condition. Only 3 samples of the

Ts65Dn-hippocampus group were considered for differential expression analysis, as one outlier was detected and removed. STRING v11 protein interaction network was used for Gene Ontology analysis. FDR<0.05 was considered for statistical significance.

Chemogenetic activation of GnRH neurons. The effect of the chemogenetic activation of GnRH neurons on cognitive and olfactory performance and LH pulsatility profile was studied according to the following procedure. Adult *Gnrh::Cre* and Ts65Dn; *Gnrh::Cre* mice were tested one month after the hM3Dq DREADD injection. For the habituation/dishabituation test, the animals received an intraperitoneal (i.p.) injection of 200μl of vehicle solution 30 min before the habituation phase. For the novel object recognition test, the animals received the same vehicle injection 30 min before the start of the trial on the first day, and 30 min before the start of the first trial on the second day. Blood sampling for LH pulsatility analysis was performed every 10 min over 120 min, 60 min before and 60 min after the injection with the vehicle solution. After a 1-month recovery period, animals were tested following the same protocol and after receiving an i.p. injection of clozapine N-oxide (CNO) (SML2304, Sigma), which activates the hM3Dq DREADD. For the behavioral tests, CNO was administered at a dose of 2 mg/kg of body weight (*105*). For the LH pulsatility analysis, CNO was administered at a dose of 1 mg/kg of body weight.

Acute GnRH injections. In order to study the effect of GnRH on cognitive and olfactory performance, both adult male Ts65Dn sham mice and mice grafted with a POA explant from *Gnrh::Cre*; *BoNTB*$^{\text{loxP-STOP-loxP}}$ double transgenic mice (*BoNTB*$^{\text{Gnrh}}$) were treated with GnRH-1 peptide (Genecust) at a dose of 50 μg/kg of body weight, or vehicle (saline 0.9%).

To test olfactory discrimination capacity, the animals received a single i.p. injection of GnRH-1 or vehicle 2h before the habituation phase. In the case of the novel object recognition test, on day 1, the animals received two i.p. injections of GnRH-1 peptide or vehicle. The first injection was given 2 h before the start of the trial, and the second one 12 hours after the first injection. On day 2, the animals received an i.p. injection of GnRH-1 peptide or vehicle 2 h before the start of the first trial.

Immunohistochemical analysis. Neonatal (P0) mice, anesthetized on ice, and infantile (P12), prepubertal (P35) and adult mice, anesthetized with 50-100 mg/kg of Ketamine-HCl and 5-10mg/kg Xylazine-HCl, were perfused transcardially with 10-100 ml of saline, followed by 10-100 ml of 4% paraformaldehyde (PFA, pH7.4). Brains were collected and fixed with the same fixative for 2h at 4°C, cryoprotected in 20% sucrose, embedded in optical cutting temperature (OCT) embedding medium (Tissue-Tek), frozen on dry ice, and stored at –80°C until use.

Tissues were cryosectioned (Leica cryostat) at 16 µm intervals for P0 and at 35 µm intervals (frozen sections were collected with a brush and placed in PBS, i.e., free-floating sections) for P12, P35 and adult brains, unless otherwise indicated.

Assessment of GnRH protein expression. Immunohistochemical labeling was carried out as previously reported (*106, 107*). Briefly, coronal sections were washed in 0.1M PBS, and incubated in blocking solution (2% goat serum + 0.5% Triton X-100) in PBS 0.1M for 60 min. Subsequently, sections were incubated in primary antibodies diluted in blocking solution for 48 h at 4°C: guinea pig anti-GnRH (1:10000) raised by Dr. Erik Hrabovszky, (Laboratory of Endocrine Neurobiology, Institute of Experimental Medicine of the Hungarian Academy of Sciences, Budapest, Hungary) (*108*) in the case of P0 brains; and rabbit anti-GnRH (1:3000), a generous gift from Prof. G. Tramu (Centre Nationale de la Recherche Scientifique, URA 339, Université Bordeaux I, Talence, France) (*109*), in the case of P12, P35 and adult brains. After incubation with primary antibodies, sections were rinsed with 0.1M PBS three times for 10 min each and then incubated Alexa Fluor 568-conjugated anti-guinea pig IgG (Life Technologies, Molecular Probes, Invitrogen, A-11075, RRID:AB_2534119) or anti-rabbit IgG (Invitrogen, A11077, RRID:AB_2534121 secondary antibodies, both at 1:500 for 90 min at room temperature. Sections were then washed, counterstained with Hoechst (1:10,000; ThermoFisher Sci #H3569, RRID:AB_2651133) for 3 min, rinsed with 0.1M PBS three times for 10 min and mounted with coverslips using Mowiol coverslip mounting solution. Because the GnRH neuronal population is very limited in the mouse brain, all neurons were counted by eye under the microscope in alternate series of brain (P12, P35 and adult) or head (P0) sections. Images were acquired using a Zeiss Axio Imager Z2 ApoTome microscope (Zeiss, Germany), as detailed in the Fluorescence Microscopy section below.

Immunohistochemical labeling of GnRHR::GFP neurons. Coronal sections were then washed in 0.1M PBS, and incubated in blocking solution (2% goat serum + 0.3% Triton X-100) in PBS 0.1M for 60 min. Subsequently, sections were incubated with chicken anti-GFP (1:1000; Aves Labs, Inc GFP-1020, RRID:AB_10000240) in 2% normal donkey serum / 0.25% BSA / 0.3% Triton X-100 incubation solution for 48 h at 4°C. After incubation in the primary antibody, sections were rinsed with 0.1M PBS three times for 10 min each and incubated with Alexa Fluor 488-AffiniPure donkey anti-chicken IgY (IgG) (1:400; Jackson ImmunoResearch Ltd.; code # 703-545-155, RRID:AB_2340375).

Assessment of Adeno-associated viral vector-mediated transduction. Coronal sections were then washed in 0.1M PBS, and incubated with blocking solution (5% donkey serum + 0.5% Triton X-100 in 0.1M PBS) for 60 min. The sections were then incubated with chicken anti-GFP (1:500; Aves Labs, Inc GFP-1020, RRID:AB_10000240) and rabbit anti-GnRH (1:3000), a generous gift from Prof. G. Tramu (Centre Nationale de la Recherche Scientifique, URA 339, Université Bordeaux I, Talence, France), in blocking solution for 48 h at 4°C. Following this, sections were rinsed with 0.1M PBS three times for 10 min each, and then incubated with the secondary antibody Alexa Fluor 488-conjugated donkey anti-chicken IgY (1:500; Jackson ImmunoResearch 703-545-155, RRID:AB_2340375) and Alexa 568 conjugated donkey anti-rabbit IgG (1:500; Invitrogen A10042, RRID:AB_2534017) for 90 min at room temperature. Sections were then washed, counterstained with Hoechst (1:10,000; Thermo Fisher Scientific Cat# H3569, RRID:AB_2651133) for 3 min, rinsed with 0.1M PBS three times for 10 min, and coverslipped using Mowiol coverslip mounting solution. Images were acquired using an LSM 710 Zeiss upright confocal laser-scanning microscope equipped with LSM 710 software (Zeiss, Germany).

Multiplex Fluorescence in situ hybridization (FISH). Adult mouse brains were fresh-frozen in dry ice and stored at -80°C until use. Tissues were cryosectioned using a CM3050 Leica Cryostat at 18 μm. FISH was performed on frozen sections of the OVLT and Hippocampus regions by RNAscope Multiplex Fluorescent Kit v2 according to the manufacturer's protocol (Advanced Cell Diagnostics). Specific probes were used to detect *gnrh1* (#476281-C3) and *otx2* (#444381-C1) mRNAs. Sections were mounted using Mowiol (Calbiochem, USA). Images were acquired using an LSM 710 confocal microscope (Zeiss) using 10X, 20X and 40X objectives. Two-three sections/animal containing the medial OVLT (rPOA) were used to assess the mean number of cells expressing *gnrh1* mRNA/OVLT section. The percentage of GnRH neurons expressing *otx2* transcripts was assessed in 2 OVLT sections per animal, genotype/treatment group by analysing 40X single plane confocal images.

iDisco. iDisco is a solvent-based clearing method that renders brain tissue transparent while preserving fluorescence (*110, 111*). *Sample pre-treatment with methanol*: Samples were washed in PBS (twice for 1 h), followed by incubation in 50% methanol in 0.1M PBS (once for 1 h), 80% methanol (once for 1 h) and 100% methanol (twice for 1 h). Next, samples were bleached in 5% H_2O_2 in 20% DMSO/methanol (2ml 30% H_2O_2/2ml DMSO/8ml methanol, ice cold) at 4°C overnight. Following this, samples were washed sequentially in methanol (twice for 1 hour), 20%

DMSO/methanol (twice for 1 h), 80% methanol (once for 1 h), 50% methanol (once for 1 h), PBS (twice for 1 h), and finally, PBS/0.2% TritonX-100 (twice for 1 h) before proceeding to the immunolabeling protocol. *Whole-mount immunolabeling*: Samples were incubated at 37°C on an adjustable rotator in 10 ml of blocking solution (PBSGNaT) [1X PBS containing 0.2% gelatin (Sigma), 0.01% Na Azide (Sigma-Aldrich) and 0.5% Triton X-100 (*21*)] for 3 nights. Samples were then rotated at 37°C for 7 days in 10 ml of PBSGNaT containing either a rabbit anti-GF (A6455, ThermoFisher, 1:10000, RRID:AB_221570), or a rabbit anti-GnRH (a generous gift from Prof. G. Tramu, University of Bordeaux, 1:3000). This was followed by six washes of 30 min each in PBSGNaT at room temperature and a final wash in PBSGNaT overnight at 4°C. Next, samples were incubated with Alexa Fluor 647-conjugated donkey anti-rabbit IgG (1:500, Jackson IP,706-605-152, RRID:AB_2492288), diluted in 10 ml PBSGNaT for 2 days at 37°C in a rotating tube. After six 30 min washes in PBSGNaT at room temperature, the samples were stored in PBS at 4°C in the dark until clearing. *Tissue clearing*: All incubation steps were performed at room temperature in a fume hood, on a tube rotator at 14 rpm covered with aluminum foil to avoid contact with light. Samples were dehydrated in a graded series (20%, 40%, 60%, 80% and 100%) of methanol (Sigma-Aldrich) diluted in H_2O for 1 h. This was followed by a delipidation step in 66% dichloromethane (DCM; Sigma-Aldrich) / 33% methanol. Methanol was then washed out with 100% DCM for 15 to 30 min. Samples were cleared in dibenzylether (DBE; Sigma-Aldrich) for 2 h at room temperature with rotation in the dark. Finally, samples were moved into fresh DBE and stored in glass tubes in the dark at room temperature until imaging. We were able to image samples, as described below, without any noticeable loss of fluorescence for up to 6 months.

Digital image acquisition

Immunohistochemically labelled samples were analyzed using one of the microscopes mentioned below. Adobe Photoshop (Adobe Systems, San Jose, CA, RRID:SCR_014199) was used to process the images. *Fluorescence microscopy*. Unless otherwise indicated, sections were analyzed using a Zeiss Axio Imager Z2 ApoTome microscope (Zeiss, Germany, equipped with a motorized stage and an AxioCam MRm camera (Zeiss, Germany). Specific beam splitter (BS), excitation (Ex) and emission (Em) wavelength settings for the visualization of the different fluorophores were as follows: green (Alexa 488-BS: 495 nm, Ex: 450/490 nm, Em: 500/550 nm), red (Alexa 688-BS: 570 nm, Ex: 538/562 nm, Em: 570/640 nm), far red (Alexa 647-BS: 660 nm, Ex: 625/655 nm, Em: 665/715 nm) and nuclear staining (Hoechst-BS: 395 nm, Ex: 335/383 nm, Em: 420/470 nm). To

create photomontages, single-plane images were captured sequentially for each fluorophore using the MosaiX module of the AxioVision 4.6 system (Zeiss, Germany) and a Zeiss 20x objective (numerical aperture NA=0.80). High magnification photomicrographs represent maximum intensity projections derived from a series of adjacent ApoTome images collected using the Z-stack module of the AxioVision 4.6 system. All images were captured in a stepwise fashion over a defined z-focus range corresponding to all visible labeling within the section and consistent with the optimal step size for the corresponding objective and wavelength.

Light sheet imaging and 3D visualization. 3D imaging was performed as previously described (*112*). An Ultramicroscope I (LaVision BioTec) using ImspectorPro software (LaVision BioTec) was used to perform imaging. The light sheet was generated by a laser (wavelength 488 or 561 nm, Coherent Sapphire Laser, LaVision BioTec) and two cylindrical lenses. A binocular stereomicroscope (MXV10, Olympus) with a 2x objective (MVPLAPO, Olympus) was used at different magnifications (1.6x, 4x, 5x, and 6.3x). Samples were placed in an imaging reservoir made of 100% quartz (LaVision BioTec) filled with DBE and illuminated from the side by the laser light at maximum sheet width. A PCO Edge SCMOS CCD camera (2,560 × 2,160 pixel size, LaVision BioTec) was used to acquire images. The step size between images was fixed at 2 µm. The resulting tiff series was converted into the Imaris file format (Imaris FileConverter, Bitplane) for 3D reconstruction, and imported into Imaris (Bitplane) for visualization, snapshots and animation.

Continuous and pulsatile subcutaneous infusion. Adult mice were implanted either with osmotic minipumps (1002, Alzet, USA) to receive a continuous infusion of vehicle (sterile 0.1M PBS) or Lutrelef (0.25 µg/ 3 h) (Ferring Pharmaceuticals, Switzerland), or with a programmable micro-infusion pump (SMP-300, iPRECIO, Japan) to receive pulsatile infusions of vehicle or Lutrelef (0.25 µg delivered over 10 min, every 3 h), mimicking the GnRH/LH pulsatility reported in WT mice (*91*), with a basal low dose infusion rate (0.0025 µg/10 min) the rest of the time. The pumps were placed under the skin on the back of the mice. Both olfactory and cognitive deficiencies were confirmed beforehand in these animals. One week after the surgery, mice were retested to evaluate their olfactory and cognitive performance. Two weeks after the surgery, repeated tail-tip blood sampling was undertaken (as described elsewhere) to assess the LH pulsatility profile.

Sample size and randomization statement. Sample sizes for physiological and neuroanatomical studies and for microRNA and gene expression analyses were estimated based on past experience and sample sizes presented in the literature. Mice from at least three different litters from each group were used to study sexual maturation and fertility and used to perform WB, quantitative RT-PCR analyses, FACS, histology and immunolabeling. No randomization method was used to assign subjects to the experimental groups or to collect and process data.

Transcriptomic analysis of GnRH signaling genes from external datasets of AD and aging. GnRH signaling pathway genes were retrieved from the Kyoto Encyclopedia of Genes and Genomes (KEGG Pathway database) using The Database for Annotation, Visualization and Integrated Discovery (DAVID) v6.8. A large-scale gene expression dataset of the post-mortem Alzheimer's disease (AD) brain was obtained from Wang *et al*. (*64*). The dataset used for this study comprised genes differentially expressed between High and Low Braak stages from the cortical areas of 125 AD patients (1053 post-mortem brain samples) (FDR<0.05). Differential expression analysis of the AD mouse model was obtained from Chatterjee *et al*. (*65*), in which the dorsal hippocampus of Thy-Tau22 mice (8 months-old) during learning was used for RNA-seq (FDR<0.05 and |log2 Fold Change|>0.2). A differential exon usage dataset associated with normal aging in the mouse CA1 hippocampal region was obtained from Benito *et al*. (*63*) (FDR<0.05). The biological database STRING (Search Tool for the Retrieval of Interacting Genes/Proteins) was used to assess predicted protein–protein interactions.

Presentation of data and statistics. All statistical analyses were performed using Prism 8 (GraphPad software) and assessed for normality (Shapiro-Wilk test) and variance, when appropriate. Sample sizes were chosen according to standard practice in the field. Statistical differences were evaluated using unpaired/paired two-tailed Student's *t*-tests for comparison of two groups and one- or two-way (repeated measures) analysis of variance (ANOVA) with Tukey's/Sidak's post hoc tests for comparison of more than two groups. When the criteria for normality or equal variance were not met, a Mann-Whitney U or Wilcoxon matched-pair test was used for the comparison of two groups and a Kruskal-Wallis with Dunn's post hoc test was used to compare more than two groups. For balanopreputial separation, vaginal opening and first ovulation, comparisons between groups were carried out using a Gehan-Breslow-Wilcoxon matched-pairs test. The significance level was set at $p < 0.05$. Data are presented as means ± S.E.M.

Open-label pilot study in patients with Down syndrome

Study Population

A pilot study on 7 DS men was conducted in the department of Endocrinology (Lausanne University Hospital - CHUV, Switzerland) to assess the effect of 6-month pulsatile GnRH therapy on cognitive and olfactory functions (clinicaltrials.gov, NCT04390646). Written informed consent was obtained from all participants and their legal representative prior to inclusion (Ethics Committee of Vaud, 2020-00270). French-speaking DS patients were between 20-50 years old, verbal, with impaired olfaction (Sniffin' Sticks, Burghart GmbH). Subjects abusing alcohol, drugs or seeking fertility were excluded. Six age- and sex-matched healthy controls were also recruited to compare baseline parameters (physical examination and blood tests).

Baseline clinical evaluation. A detailed history and physical examination were performed. Fasting morning blood samples were collected to measure: (i) serum levels of LH and FSH before and after GnRH test (100 ug iv LHRH Ferring Pharmaceuticals) (*113*), testosterone, estradiol, and inhibin B; (ii) serum glucose, insulin, lipids, leptin, ASAT, ALAT, and high sensitivity CRP (hsCRP) levels; (iii) homocysteine levels (*114*) and neurofilament light chain (Nfl) (*44*). Methodology for laboratory assays can be found in Supplementary methods. Cognitive abilities were assessed after breakfast using the Montreal Cognitive Assessment (MoCA) (*115*), with a cutoff for cognitive impairment < 26, and the Token test (*116*) exploring verbal comprehension < 28. Detailed olfactory evaluation was performed using the Sniffin' Sticks Extended tests including three subtests (odor threshold, discrimination, and identification) (*117*). Quality of life questionnaire was assessed using the 12-item short-form health survey (*118*).

Pulsatile GnRH treatment. Pulsatile GnRH therapy (Lutrelef®, Ferring SA, Switzerland) was given for 6 months via a subcutaneous pump at a rate of 75 ng/kg/pulse at 2-hr intervals to mimic the LH pulse frequency observed in normal men (*41*) (LutrePulse® manager and LutrePod®, Ferring SA, Switzerland). The dose of 75 ng/kg/pulse was chosen as it is the average dose given to GnRH deficient men to achieve normal reproductive function (*119*). The primary efficacy end-point was changes in the total MoCA score. Baseline clinical, biochemical and cognitive assessments were repeated on the last day of pulsatile GnRH therapy.

Immunoassays. Plasma testosterone was measured by chemiluminescent microparticle immunoassay (CMIA) on the Architect analyzer (Abbott), detection range was 0.05-35.0 nmol/L, limit of quantification (LOQ) was 0.1nmol/L, intra-assay coefficient of variation (CV) was 2.5-5.1%, and inter-assay CV was 3.8-7.1%. Plasma LH, FSH, and E2 were measured by electrochemiluminescence immunoassay (ECLIA) on a Cobas analyzer (Roche). Detection range was 0.3-200 IU/L for LH and FSH and 0.02-11.00 nmol/L for E2; LOQ was 0.3 IU/L for LH and FSH and 0.02 nmol/L for E2; intra-assay CV were 1.4-2.1% for LH, 0.8-2.0% for FSH, and 1.6%-8.4% for E2; inter-assay CV were 2.0-2.2% for LH, 2.6-3.2% for FSH, 1.2-3.3% for E2. Serum inhibin-B was measured by enzyme immunoassay (Cerba Laboratoire, Paris), detection range was 2.9-1000 pg/mL with a LOQ at 15 pg/mL, intra-assay CV was 3.2-4.8%, and inter-assay CV was 5.7-9.0%. Serum levels of total, LDL- and HDL-cholesterol, triglycerides, ASAT, ALAT, and high-sensitivity CRP were also measured on a Cobas analyzer (Roche). Leptin levels were measured by enzyme-linked immunosorbent assay (ELISA), detection range was 0.25-1000 μg/L with a LOQ at 0.1 nmol/L, intra-assay CV was 4.7-5.2%, and inter-assay CV was 6.4-8.2%. Homocysteine levels were determined by high-performance liquid chromatography, detection range was 1.3-200.0 μmol/L with a LOQ at 3.0 nmol/L, and inter-assay CV 2.5-3.1%. Serum neurofilament light chain (sNfL) was measured at 4-fold dilution in duplicate determination with an average CV of 3.2% with the NF-light Simoa assay (Quanterix, Billerica, MA, USA) at Prof Kuhle's laboratory at the University Hospital of Basel (*44*); sNfL assay limit of detection and quantification were 0.038 pg/mL and 0.174 pg/mL, respectively; intra-assay CV for sNfL was 1.2-6.9%.

***Statistical analyses*.** Clinical data were analyzed using GraphPad Prism 9 (GraphPad Software, USA). Shapiro–Wilk statistical test was used to assess the distribution of variables. For normally distributed quantitative variables, paired two-tailed Student's t-test was performed. Mann–Whitney test or Wilcoxon matched-pair test was used to analyze non-parametric data. Data are presented as means ± S.E.M. A p value < 0.05 is considered significant. All statistical data supporting the findings are available within the article, supplementary information files and Table S7.

Imaging studies

Structural MRI. Eight DS patients and 44 healthy age- and sex-matched controls were imaged for the baseline studies. Brain imaging data were acquired on a 3T whole-body MRI system using 64-channel radiofrequency (RF) head and body coil for transmission (Magnetom Prisma, Siemens Medical Systems, Germany). A quantitative relaxometry protocol was used, consisting of three spoiled multi-echo 3D fast low-angle shot (FLASH) acquisitions with T1-, proton density- and magnetization transfer weighting at 1 mm isotropic resolution (*120*) and of an additional acquisition to map spatial inhomogeneities of the RF transmit field B1+ (*121, 122*). Quantitative maps of proton density (PD), longitudinal relaxation rate (R1), transversal relaxation rate R2* and magnetization transfer (MT) saturation were calculated from the raw MRI data as described previously (*120, 123, 124*), using the hMRI toolbox (*125*) running under Matlab 2017a (Mathworks, Sherborn, MA, USA). To minimize image degradation due to patient motion during the acquisition of the MRI data, a prospective correction system was used (KinetiCor, HI, Honolulu) that allows the adjustment of the MRI scanner in real-time during image acquisition according to the patient's head position (*126, 127*). Furthermore, automatic suspension of data acquisition during periods of excessive head movement was also used to further minimize the impact of patient motion on image quality (*128*). The values of the Motion Degradation Index of the MT-, PD- and T1-weighted images ranged from 3.5 to 5.6, 3.1 to 4.2 and 3.2 to 4.1 s^{-1} respectively, reflecting high-quality data (*129*), except one MT-weighted (7.4 s^{-1}) and one PD-weighted (5.3s^{-1})scan.

Longitudinal data pre-processing. Seven DS patients who completed 6 month GnRH therapy were evaluated for the longitudinal study. We used the longitudinal diffeomorphic toolbox (*130*) of SPM12 (Wellcome Centre for Human Neuroimaging, London, UK; https://www.fil.ion.ucl.ac.uk/spm/) that we adapted to the multiparameter data as previously described (*131*). For the voxel-based morphometry (VBM) analysis the spatial registration procedure included scaling the grey matter tissue probability maps by the Jacobian Determinant of the deformation field (i.e. "modulation") obtained in the diffeomorphic step followed by spatial smoothing with an isotropic Gaussian smoothing kernel of 8 mm full-width-at-half-maximum (FWHM). For the voxel-based quantification (VBQ) analysis we used the previously described "weighted-averaging" procedure, which registers tissue-specific MPMs to MNI space while

preserving the total of parameter values within each tissue class (*132*).

Statistical analysis (Structural MRI). All statistical analyses were performed at the voxel level in the General Linear Model framework of SPM12. For the group comparison at baseline, we tested patients with DS (n=8) against age-matched male controls (n=44). The total intracranial volume defined as sum between grey matter, white matter and cerebro-spinal fluid volume was used as confounding variable in the VBM analysis. The association between GnRH-induced changes of global cognition and brain anatomy over time (n=7) was tested using a simple regression model for the rate of brain features change between t1 and t2. Here, we included the baseline MoCA score next to the MoCA difference between t1 and t2. For all tests we decided for a small volume correction with search volume defined by the contrast- and brain compartment- specific results from the baseline comparison with healthy controls.

Resting-state functional MRI. Acquisition of fMRI data was conducted using a custom-made 2D echo-planar imaging (EPI) sequence (*133*) that allowed for real-time correction of patient's head movement during image acquisition (KinetiCor, HI, Honolulu) (*126, 127*). The slice repetition time [TR] was 66 ms, the echo time [TE] was 30 ms, the excitation flip angle was 90º, the field of view was 192 mm and the slice thickness of 2.5 mm (inter-slice gap, 0.5 mm). Forty-nine interleaved slices were prescribed parallel to the anterior-posterior commissure line covering the whole-brain. A 10-min continuous resting-state scan was acquired for each participant. Participants were instructed to relax lying without moving and to stay awake, while keeping their eyes open throughout the test.

Rs-fMRI analyses were performed with the CONN toolbox (www.nitrc.org/projects/conn, RRID:SCR_009550) to proceed default preprocessing and to explore statistical connectivity between brain regions.

Supplementary Figures

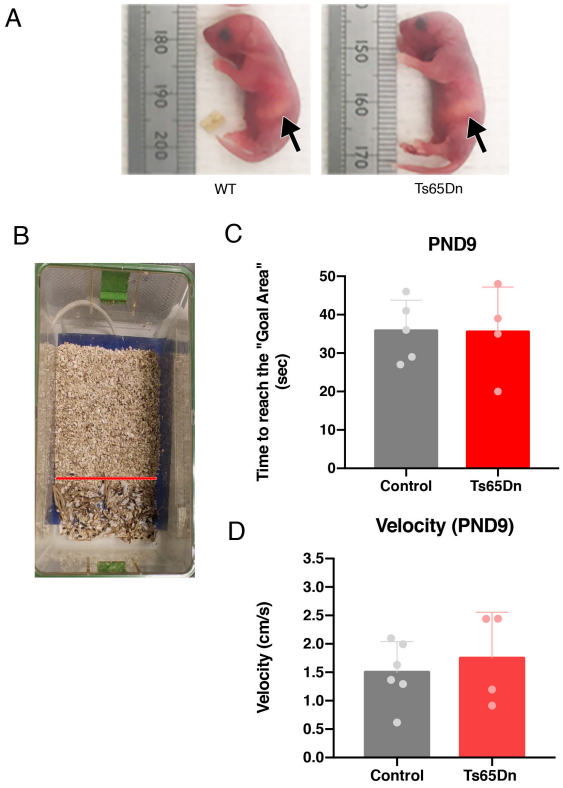

Fig. S1. T65Dn mice show normal olfaction during the neonatal and infantile periods. (**A**) Representative photographs showing that at birth, Ts65Dn pups present a comparable amount of milk in the stomach (arrow) to WT littermates. (**B-C**) Homing test showing comparable ability of T65Dn P9 pups to reach the area soiled by familiar bedding as their control littermates. (**D**) Ts65DN and WT infantile mice show also comparable locomotor activity.

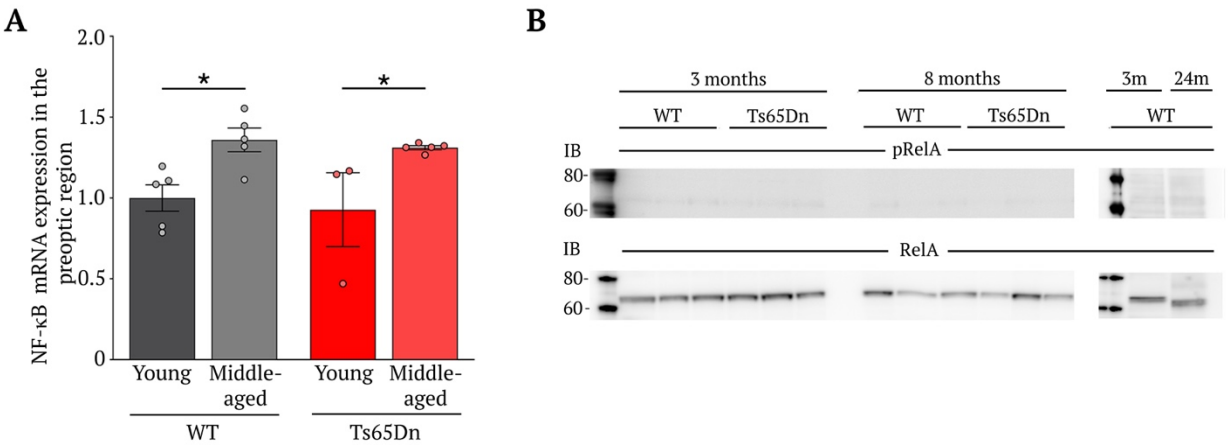

Fig. S2. Age-related expression of NF-kB in WT and trisomic littermates. (**A**) Real time PCR analysis shows an increase in the expression of Nf-κB1 transcripts in the preoptic area of the hypothalamus in middle-aged male mice (8-12 months of age) when compared to young adults (3 months of age). Values represent means ± SEM. Statistical differences were tested using an unpaired Student's *t*-test or Mann-Whitney U test. (WT young vs. WT middle-aged, $t_{(8)} = 3.27$, $P = 0.01$, n = 5 and 5; Ts65Dn young vs. Ts65Dn middle-aged, $U = 0$, $P = 0.04$, n = 3 and 5; WT young vs. Ts65Dn young, $U = 7$, $P > 0.99$, n = 5 and 3; WT middle-aged vs. Ts65Dn middle-aged, $t_{(8)} = 0.65$, $P = 0.54$, n = 5 and 5). * $P<0.05$. (**B**) Western blot analyses of the phosphorylated or activated form of RelA, which forms a dimer with Nf-κB, reveal an absence of Nf-κB/RelA transcription factor complex activation in the hippocampus of both 3- and 8-month-old WT and Ts65Dn mice.

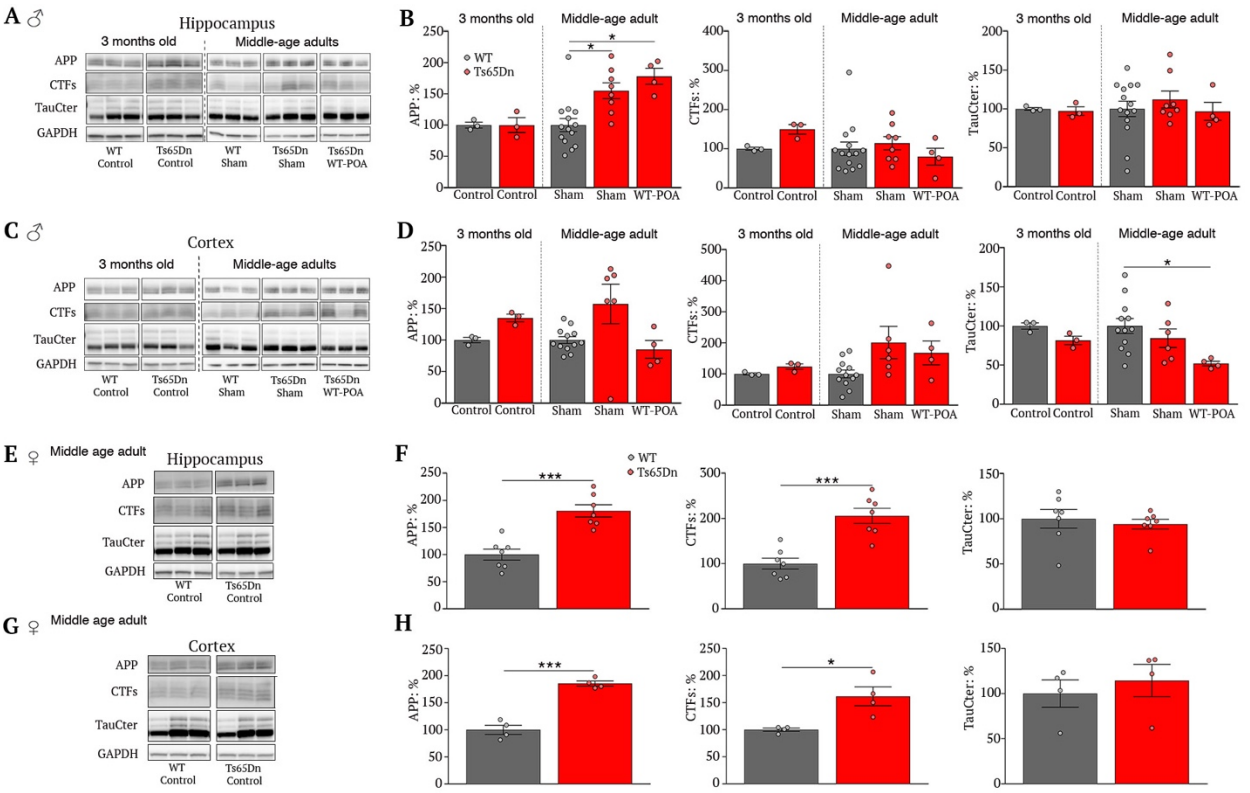

Fig. S3. Hippocampal and cortical APP, CTF and Tau-Cter expression levels in Ts65Dn mice. (A,C) Representative WBs showing hippocampal and cortical APP, CTF and Tau-Cter levels in 3-month old and middle-aged adult male Ts65Dn or WT mice (8-12-months), either grafted with POA cell suspensions from WT mice (WT-POA) or ungrafted (Sham) mice. GAPDH was used as a loading control. **(B,D)** Quantification of protein levels of APP, CTF and Tau-Cter in the hippocampus **(B)** and cortex **(D)** of male WT and Ts65Dn mice. Values represent means ± SEM. Statistical differences were tested using the Mann-Whitney U test when comparing two conditions, and a Kruskal-Wallis or one-way ANOVA when comparing three or more conditions. (**B**: WT young APP vs. Ts65Dn young APP, $U = 4$, $P > 0.99$, $n = 3$ and 3; WT Sham middle-aged APP vs. Ts65Dn Sham middle-aged APP, $Z = 2.72$, $P = 0.02$, n=14 and 8; WT Sham middle-aged APP vs. Ts65Dn WT-POA middle-aged APP, $Z = 2.82$, $P = 0.01$, $n = 14$ and 4; Ts65Dn Sham middle-aged APP vs. Ts65Dn WT-POA middle-aged APP, $Z = 0.64$, $P > 0.99$, $n = 8$ and 4; WT young CTFs vs. Ts65Dn CTFs, $U = 0$, $P = 0.10$, $n = 3$ and 3; WT Sham middle-aged CTFs vs. Ts65Dn Sham middle-aged CTFs, $Z = 1.01$, $P = 0.94$, $n = 14$ and 8; WT Sham middle-aged CTFs vs. Ts65Dn WT-POA middle-aged CTFs, $Z = 0.40$, $P > 0.99$, $n = 14$ and 4; Ts65Dn Sham middle-aged CTFs vs. Ts65Dn WT-POA middle-aged CTFs, $Z = 1.09$, $P = 0.82$, $n = 8$ and 4; WT young TauCter vs. Ts65Dn young TauCter, $U = 3$, $P = 0.70$, $n = 3$ and 3; WT Sham middle-aged TauCter vs. Ts65Dn Sham middle-aged TauCter, $Z = 0.38$, $P > 0.99$, $n = 14$ and 8; WT Sham middle-aged TauCter vs. Ts65Dn WT-POA middle-aged TauCter, $Z = 0.71$, $P > 0.99$, $n = 14$ and 4; Ts65Dn Sham middle-aged TauCter vs. Ts65Dn WT-POA middle-aged TauCter, $Z = 0.9341$, $P>0.99$, n=8 and 4. **D**: WT young APP vs. Ts65Dn young APP, U=0,) $P = 0.10$, $n = 3$ and 3; WT Sham middle-aged APP vs. Ts65Dn Sham middle-aged APP, $Z = 2.03$, $P = 0.13$, $n = 12$ and 6; WT Sham middle-aged APP vs. Ts65Dn WT-POA middle-aged APP, $Z = 0.80$, $P > 0.99$, $n = 12$ and 4; Ts65Dn Sham middle-aged APP vs. Ts65Dn WT-POA middle-aged APP, $Z = 2.29$, $P = 0.07$, n=6 and 4; WT young CTFs vs. Ts65Dn young CTFs, $U = 1$, $P = 0.20$, $n = 3$ and 3; WTSham middle-aged CTFs vs. Ts65Dn Sham middle-aged CTFs, $Z = 2.39$, $P = 0.05$, $n = 12$ and 6; WT Sham middle-aged CTFs vs. Ts65Dn WT-POA middle-aged CTFs, $Z = 1.67$, $P = 0.29$, $n = 12$ and 4; Ts65Dn Sham middle-aged CTFs vs. Ts65Dn WT-POA middle-aged CTFs, $Z = 0.36$, $P > 0.99$, $n = 6$ and 4; WT young TauCter vs. Ts65Dn young TauCter, $U = 0$, $P = 0.10$, $n = 3$ and 3; WT Sham middle-aged TauCter vs. Ts65Dn Sham middle-aged TauCter, $q_{(19)} = 1.49$, $P = 0.55$, n =

12 and 6, WT Sham middle-aged TauCter vs. Ts65Dn WT-POA middle-aged TauCter, $q_{(19)} = 3.98$, $P = 0.03$, n = 12 and 4; Ts65Dn Sham middle-aged TauCter vs. Ts65Dn WT-POA middle-aged TauCter, $q_{(19)} = 2.41$, $P = 0.23$, n = 6 and 4). * $P < 0.05$. **(E,G)** Representative WBs showing hippocampal and cortical APP, CTF and Tau-Cter levels in 3-month old and middle-aged adult (12-month old) female Ts65Dn mice. GAPDH was used as a loading control. **(F,H)** Quantification of protein levels of APP, CTF and Tau-Cter in the hippocampus **(F)** and cortex **(H)** of female WT and Ts65Dn mice. GAPDH was used as a loading control. Values represent means ± SEM. Statistical differences were tested using an unpaired Student's t-test. (**F**: WT middle-aged APP vs. Ts65Dn middle-aged APP, $t_{(12)} = 5.30$, $P = 0.0002$, n = 7 and 7; WT middle-aged CTFs vs. Ts65Dn middle-aged CTFs, $t_{(12)} = 5.13$, $P = 0.0003$, n = 7 and 7; WT middle-aged TauCter vs. Ts65Dn middle-aged TauCter, $t_{(12)} = 0.51$, $P = 0.62$, n = 7 and 7. **H**: WT middle-aged APP vs. Ts65Dn middle-aged APP, $t_{(6)} = 8.92$, $P = 0.0001$, n=4 and 4; WT middle-aged CTFs vs. Ts65Dn middle-aged CTFs, $t_{(6)} = 3.48$, $P = 0.01$, n = 4 and 4; WT middle-aged TauCter vs. Ts65Dn middle-aged TauCter, $t_{(6)} = 0.6140$, $P = 0.56$, n = 4 and 4). $P < 0.05$; *** $P < 0.001$.

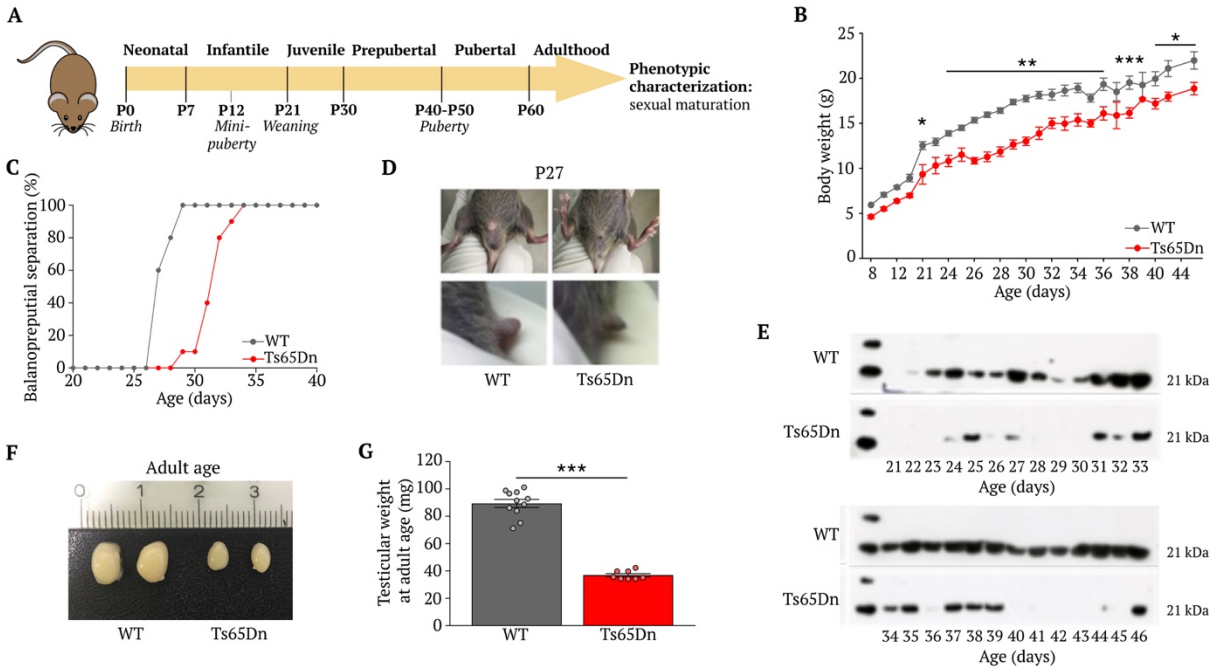

Fig. S4. Male Ts65Dn mice show delayed sexual maturation and hypogonadism. (**A**) Schematic representation illustrating the phenotypic characterization of reproductive maturation performed in Ts65Dn mice from birth to the adulthood. (**B**) Ts65Dn males presented significantly lower body weight gain during postnatal development. Values represent means ± SEM. Statistical differences were tested using a two-way repeated measures ANOVA. (Time factor, $F_{(24,211)} = 191.8$, $P < 0.0001$; Column factor, $F_{(1,22)} = 68.18$, $P < 0.0001$, Time x column factor, $F_{(24,211)} = 3.33$, $P < 0.0001$). * $P < 0.05$; ** $P < 0.01$; *** $P < 0.001$. (**C-E**) A marked delay in sexual maturation was observed in male Ts65Dn mice compared with WT littermates. Ts65Dn males exhibited delayed balanopreputial separation day (C), a smaller penis and undescended testes (**D**); all external signs used to follow sexual maturation. (**E**) Ts65Dn mice showed an irregular expression profile of major urinary proteins. Values represent the cumulative percentage of subjects that achieved a given state. Statistical differences were tested using a Gehan-Breslow-Wilcoxon matched-pair test. (WT vs. Ts65Dn, $\chi^2_{(1)}(1) = 17$, $P < 0.0001$, n = 10 and 10). ****$P < 0.0001$. (**F,G**) Adult Ts65Dn males revealed severe hypogonadism, exhibiting smaller testes and lower testicular weight. Values represent means ± SEM. Statistical differences were tested using a Mann-Whitney U test. (WT vs. Ts65Dn, U = 0, $P < 0.0001$, n = 11 and 8). *** $P < 0.001$.

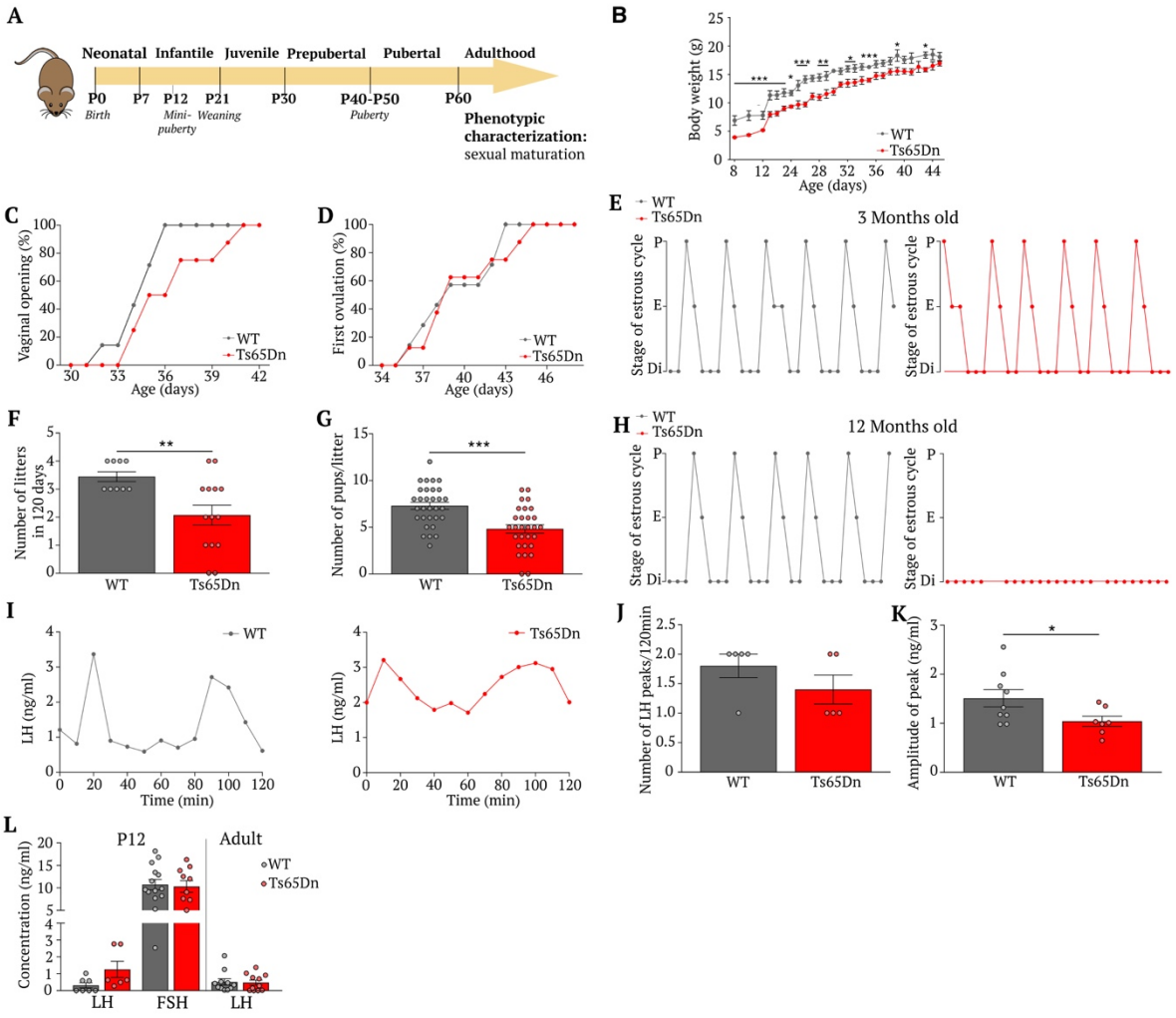

Fig. S5. Ts65Dn female mice show normal sexual maturation but subfertility and precocious ovarian failure. (**A**) Schematic representation illustrating the phenotypic characterization of reproductive maturation in Ts65Dn mice from birth to adulthood. (**B**) Ts65Dn females display significantly lower body weight gains during postnatal maturation and the pubertal transition. Values represent mean ± SEM. Statistical differences were tested using a two-way repeated measures ANOVA. (Time factor, $F_{(26,256)} = 164$, $P < 0.0001$; Column factor, $F_{(1,32)} = 32.88$, $P < 0.0001$; Time x Column Factor, $F_{(26,256)} = 1.27$, $P = 0.18$). * $P < 0.05$; **$P < 0.01$; *** $P < 0.001$. (**C,D**) Normal sexual maturation is observed in female Ts65Dn mice compared with wt littermates. Values represent the cumulative percentage of subjects that achieved a given state. Statistical differences were tested using a Gehan-Breslow-Wilcoxon matched-pairs test. (**C**: WT vs. Ts65Dn, $\chi^2_{(1)} = 2.05$, $P = 0.15$, n = 7 and 8. **D**: WT vs. Ts65Dn, $\chi^2_{(1)} = 0.12$, $P = 0.73$, n = 7 and 8). (**E**) Representative oestrous cyclicity of 3-month old wt and Ts65Dn females over 28 consecutive days. (**F,G**) Adult Ts65Dn females are subfertile, showing fewer litters produced over a 120-day period and fewer pups per litter. Values represent means ± SEM. Statistical differences were tested using an unpaired Student's *t*-test or Mann-Whitney U test. (**F**: WT vs. Ts65Dn, U = 24, $P = 0.01$, n = 9 and 14. **G**: WT vs. Ts65Dn, $t_{(58)} = 4.23$, $P = 0.00008$, n = 31 and 29). ** $P < 0.01$; ** $P < 0.001$. (**H**) Representative oestrous cyclicity of middle-aged (12-month old) WT and Ts65Dn female

mice. Di, diestrus, P, proestrus; E, oestrus. (**I**) Representative graphs for LH pulsatility assessment by serial blood sampling in WT (left panel) and Ts65Dn females (right panel). Ts65Dn mice show normal LH pulse frequency (**J**) but decreased LH pulse amplitude (**K**). Values represent means ± SEM. Statistical differences were tested using an unpaired Student's *t*-test or Mann-Whitney U test. (**J**: WT vs. Ts65Dn, U = 7.5, $P = 0.52$, n = 5 and 5. **K**: WT vs. Ts65Dn, $t_{(14)} = 2.16$, $P = 0.49$, n = 9 and 7). * $P < 0.05$. (**L**) Circulating levels of the gonadotropins LH and FSH at P12 and in adults were similar in wt and Ts65Dn females. Values represent means ± SEM. Statistical differences were tested using an unpaired Student's *t*-test or a two-way repeated measures ANOVA (wt LH P12 vs. Ts65Dn LH P12, U = 8, $P = 0.06$, n = 7 and 6; WT FSH P12 vs. Ts65Dn FSH P12, $t_{(22)} = 0.23$, $P = 0.82$, n=14 and 10; WT LH adult vs. Ts65Dn LH adult, U = 53, $P = 0.64$, n = 11 and 11).

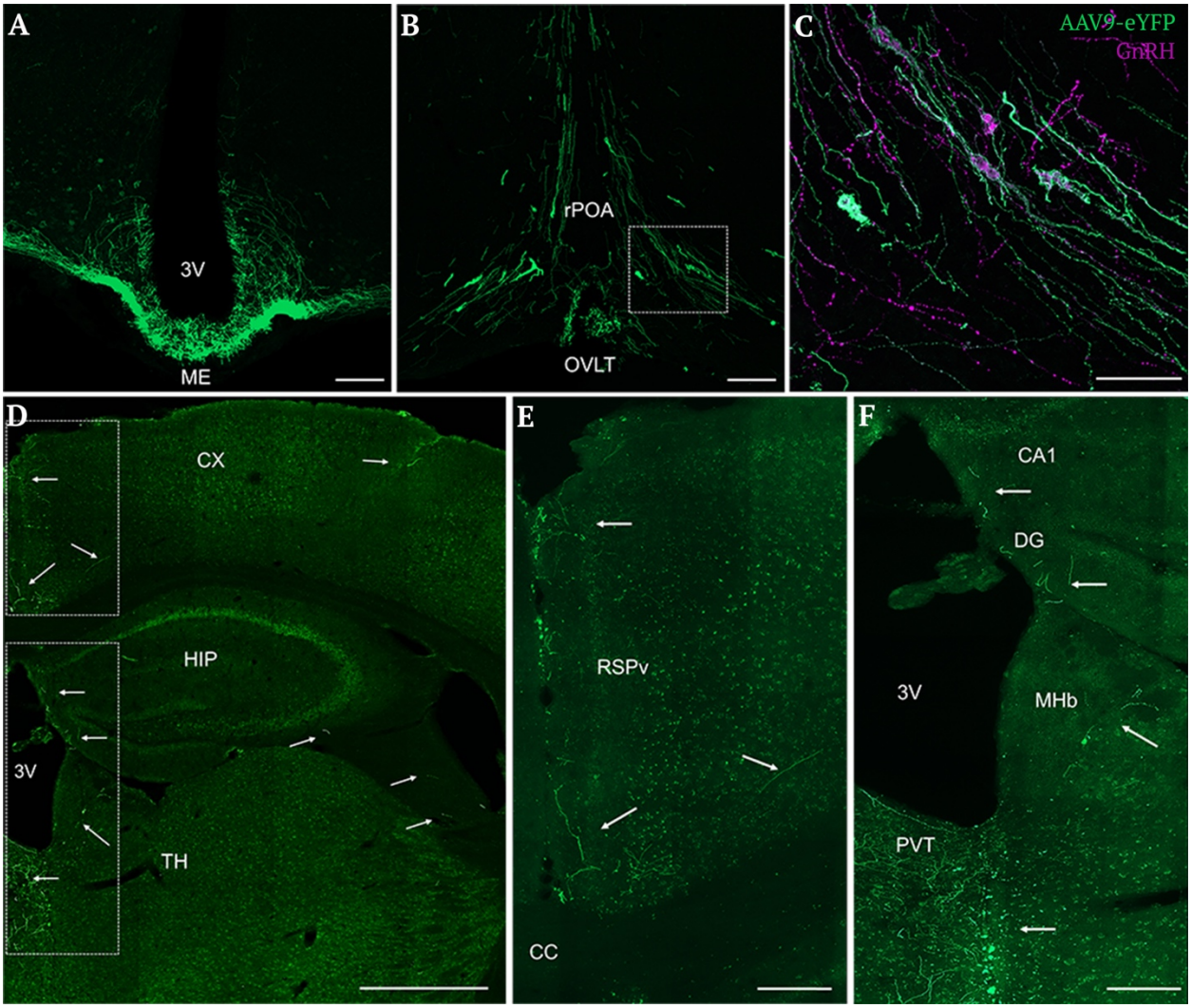

Fig. S6. Innervation of extrahypothalamic regions by hypophysiotropic GnRH neurons in adult mice. (**A**) Cre-dependent viral tracing from the median eminence (ME) showing the expression of eYFP (green) in hypophysiotropic GnRH neurons of *GnRH::Cre* male mice. Scale bar: 100 μm. (**B**) A single injection of AAV9-eYFP in the dorsolateral part of the ME induces the expression of eYFP in GnRH neurons located in the rostral preoptic area (rPOA) and in the organum vasculosum laminae terminalis (OVLT). Scale bar: 100 μm. (**C**) Higher magnification of the box in **B** showing colocalization between virally induced eYFP expression and immunolabeling for GnRH (magenta) in the rPOA. Scale bar: 50 μm. (**D**) Visualization of AAV9-eYFP-expressing GnRH neuron fibres in the cortex (CX), hippocampus (HIP) and thalamus (TH). Scale bar: 500 μm. (**E**) High magnification image showing the presence of AAV9-eYFP-transduced GnRH neuronal fibres reaching the ventral layer of the retrosplenial (RSPv) region of the cortex. Scale bar: 100 μm. (**F**) High magnification image showing AAV9-eYFP-transduced GnRH neuronal fibres in the dentate gyrus (DG) and CA1 region of the HIP, the medial habenula (MHb) and the paraventricular thalamus (PVT). Scale bar: 100 μm. 3V, third ventricle. CX, cortex. CA, cornu ammonis. CC, corpus callosum. DG, dentate gyrus. HIP, hippocampus. ME, median eminence. MHb, medial habenula. OVLT, organum vasculosum laminae terminalis. PVT, paraventricular thalamus. rPOA, rostral preoptic area. TH, thalamus.

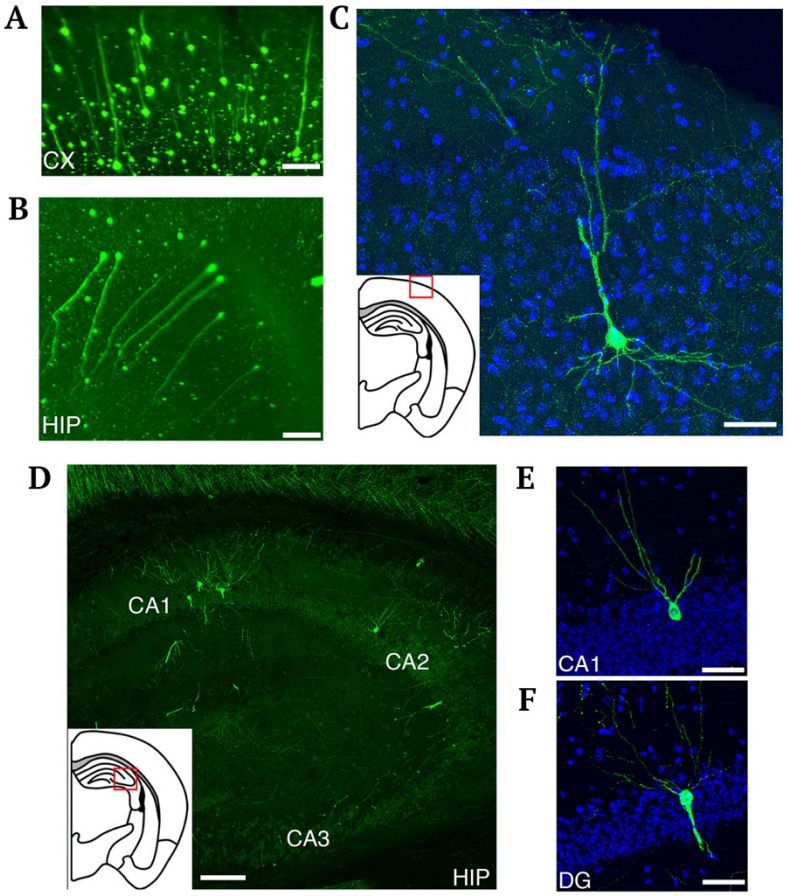

Fig. S7. GnRHR expressing cells in the neocortex of *Gnrhr::Cre*;*Tau*^{GFP} mice and GnRH neuronal cell body distribution at birth in Ts65Dn and wild-type littermates. (**C-F**) Confocal microscopy of GFP-labeled GnRHR-expressing cells in the cortex (**A, C**) and in the dentate gyrus (DG) and CA1-3 regions of the hippocampus (**B, D-F**). CX, cortex. CA, cornu ammonis. DB, diagonal band of Broca. DG, dentate gyrus. HIP, hippocampus. ME, median eminence. MEAad, anteriodorsal amygdala. MS, medial septal nucleus. OB, olfactory bulb. OV, organum vasculosum. PVT, paraventricular thalamus. Scale bars: **A,B,** 50 μm; **C,** 30 μm; **D,** 80 μm; **E,F**, 10 μm.

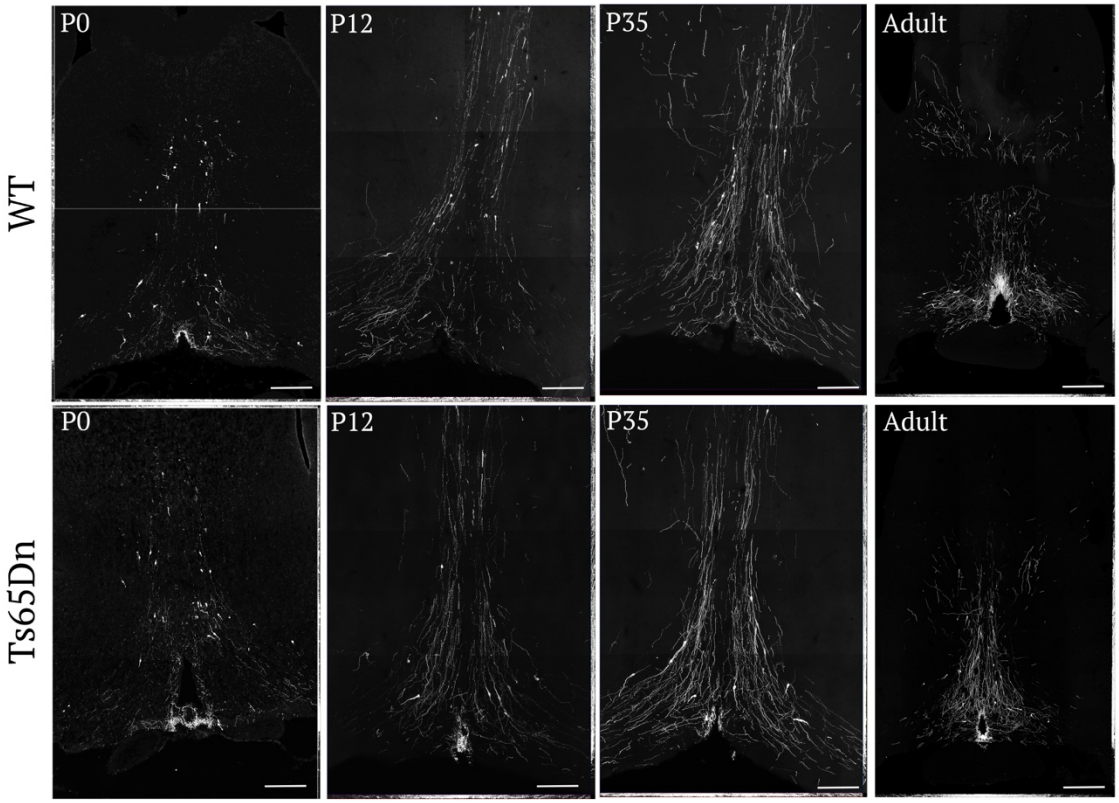

Fig. S8. Ts65Dn mice show an age-dependent loss of GnRH immunoreactivity. Representative photomicrographs of GnRH immunoreactivity taken from male Ts65Dn and WT littermate mice at different ages of postnatal development: neonatal (P0), minipubertal (P12), prepubertal (P35) and adult. Scale bars: 200 μm.

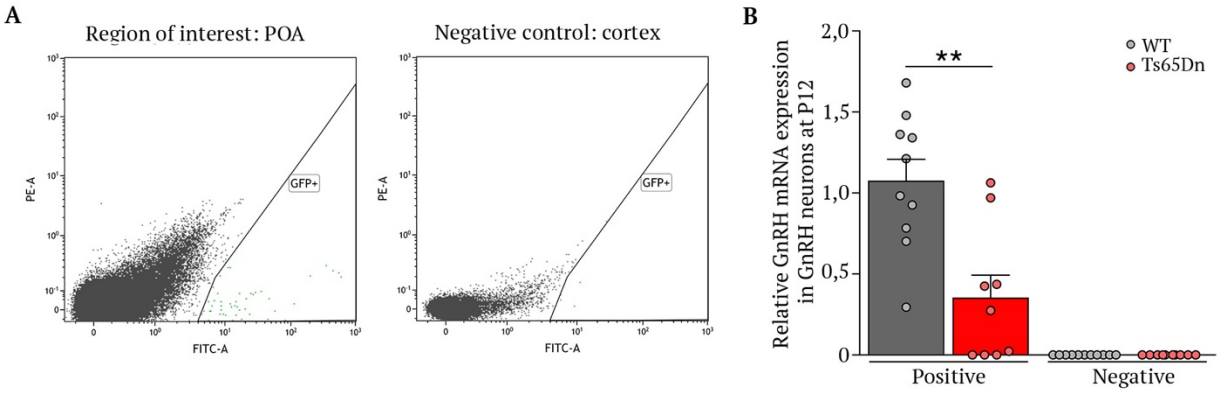

Fig. S9. Isolation of hypothalamic GnRH neurons in postnatal mice. (**A**) Isolation of GnRH-GFP-positive neurons from the preoptic area (POA) by FACS. The cortex was used as a negative control. (**B**) Real-time PCR analysis of GnRH mRNA expression in GFP-positive and negative cells. Values represent means ± SEM. Statistical differences were tested using a Mann-Whitney U test. (Positive cells: WT vs. Ts65Dn, U = 11, $P = 0.004$, n =10 and 9; Negative cells: WT vs. Ts65Dn, U = 52, $P = 0.86$, n = 11 and 10). ** $P<0.01$.

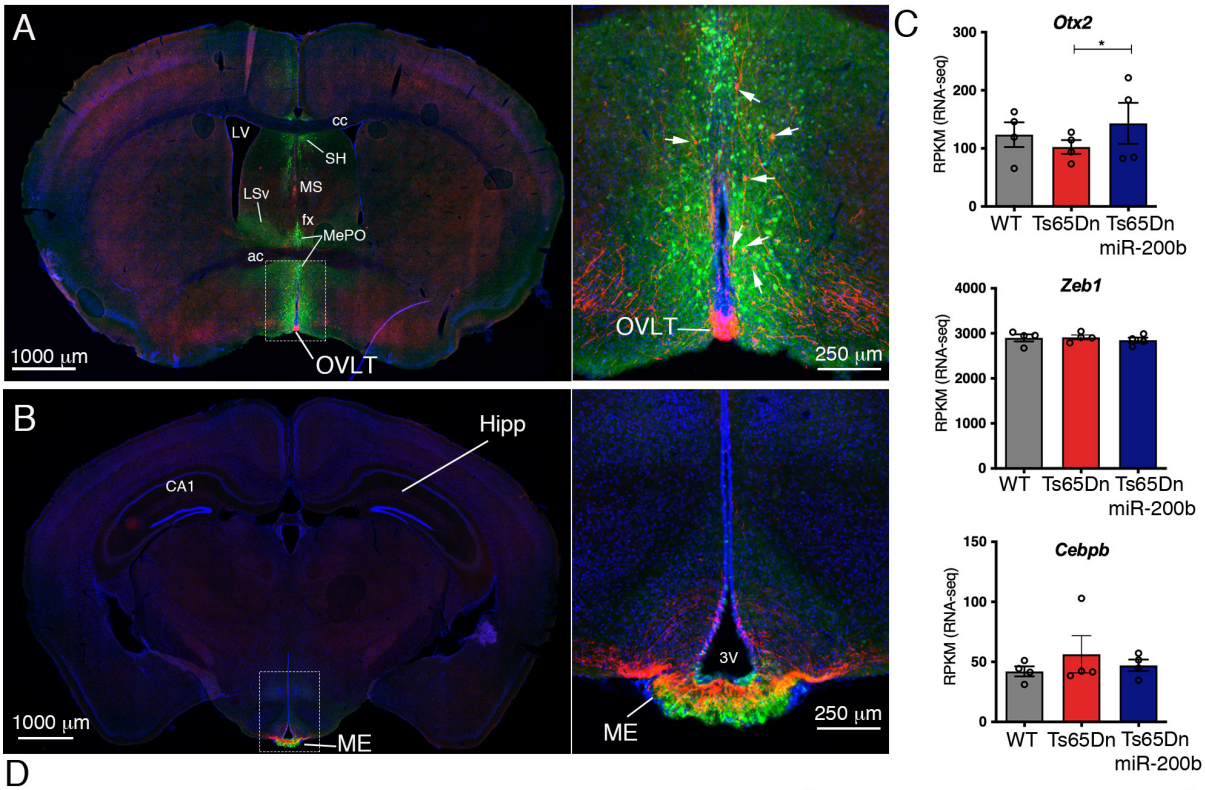
A
LV
cc
SH
MS
LSv
fx
MePO
ac
OVLT
1000 μm
OVLT
250 μm
B
Hipp
CA1
1000 μm
ME
3V
ME
250 μm
C
Otx2
RPKM (RNA-seq)
300
200
100
0
*
WT
Ts65Dn
Ts65Dn miR-200b
Zeb1
RPKM (RNA-seq)
4000
3000
2000
1000
0
WT
Ts65Dn
Ts65Dn miR-200b
Cebpb
RPKM (RNA-seq)
150
100
50
0
WT
Ts65Dn
Ts65Dn miR-200b
D
WT
Ts65Dn
Ts65Dn miR-200b
Gnrh1 Otx2
OVLT
OVLT
OVLT
200 μm
Gnrh1

Fig. S10. Spreading of AAV-miR200b-eGFP infection and its effect on the expression of *Gnrh1* promoter modulators. (**A**,**B**) Representative eGFP-immunolabeling showing that most of the miR-200b-expressing AAV stays mostly confined to the preoptic-septal region (**A**) and the median eminence (ME), to which GnRH neurons (red, arrows) project (**B**), two weeks after infection. Insets show higher magnification of the areas framed in (**A**) and (**B**). (**C**) Overexpression of miR-200b in the preoptic region results in the abundance of *Otx2*, but not *Zeb1* and *Cebpb* transcripts compared to overall gene expression (RPKM values) in the preoptic region in Ts65Dn mice (n=4 male littermates per group from more than 3 litters). (**D**) Representative fluorescent *in situ* hybridization images showing the upregulation of both *Otx2* and *Gnrh1* transcripts in adult Ts65Dn male mice overexpressing miR-200b in the preoptic region. OVLT: organum vasculosum laminae terminalis; MePO: median preoptic nucleus; LSv: lateral septal nucleus ventral part; MS: medial septal nucleus; SH: septohippocampal nucleus; Hipp: hippocampus; LV: lateral ventricle; 3V: third ventricle; ac: anterior commissure; cc: corpus callosum; fx: fornix.

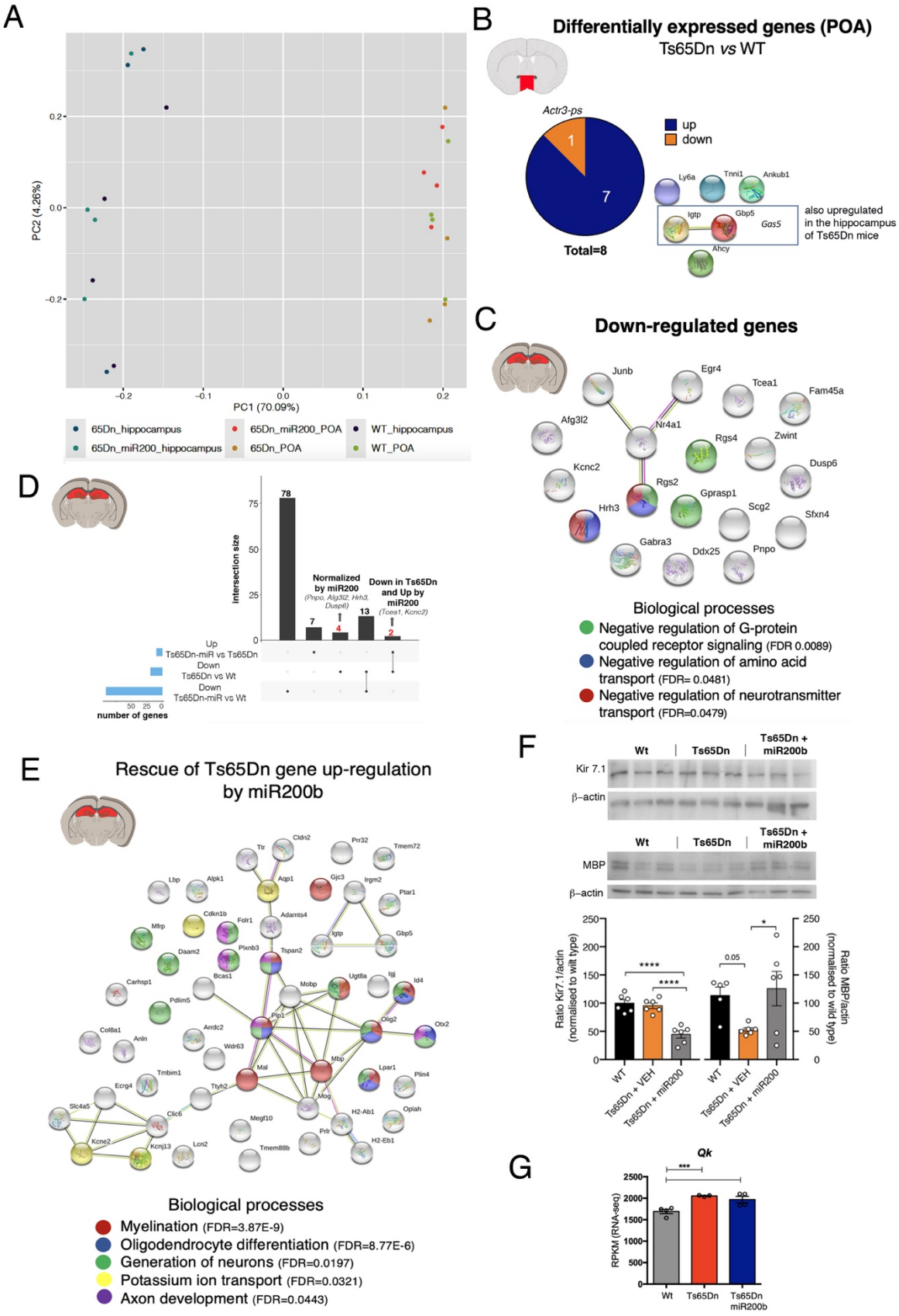
A
PC2 (4.26%)
PC1 (70.09%)
65Dn_hippocampus
65Dn_miR200_hippocampus
65Dn_miR200_POA
65Dn_POA
WT_hippocampus
WT_POA
B
Differentially expressed genes (POA)
Ts65Dn vs WT
Actr3-ps
up
down
Total=8
Ly6a
Tnni1
Ankub1
Igtp
Gbp5
Gas5
Ahcy
also upregulated in the hippocampus of Ts65Dn mice
C
Down-regulated genes
Junb
Egr4
Tcea1
Fam45a
Afg3l2
Nr4a1
Rgs4
Zwint
Kcnc2
Rgs2
Gprasp1
Dusp6
Hrh3
Scg2
Sfxn4
Gabra3
Ddx25
Pnpo
Biological processes
Negative regulation of G-protein coupled receptor signaling (FDR 0.0089)
Negative regulation of amino acid transport (FDR= 0.0481)
Negative regulation of neurotransmitter transport (FDR=0.0479)
D
intersection size
78
7
4
13
2
Normalized by miR200
(Pnpo, Afg3l2, Hrh3, Dusp6)
Down in Ts65Dn and Up by miR200
(Tcea1, Kcnc2)
Up
Ts65Dn-miR vs Ts65Dn
Down
Ts65Dn vs Wt
Down
Ts65Dn-miR vs Wt
number of genes
E
Rescue of Ts65Dn gene up-regulation by miR200b
Biological processes
Myelination (FDR=3.87E-9)
Oligodendrocyte differentiation (FDR=8.77E-6)
Generation of neurons (FDR=0.0197)
Potassium ion transport (FDR=0.0321)
Axon development (FDR=0.0443)
F
Wt
Ts65Dn
Ts65Dn + miR200b
Kir 7.1
β-actin
MBP
β-actin
Ratio Kir7.1/actin (normalised to wilt type)
Ratio MBP/actin (normalised to wild type)
WT
Ts65Dn + VEH
Ts65Dn + miR200
G
Qk
RPKM (RNA-seq)
Wt
Ts65Dn
Ts65Dn miR200b

Fig. S11. Transcriptomics of Ts65Dn mice and its rescue by miR200b overexpression in the preoptic region. (**A**) Principal component analysis (PCA) plot showing the distribution of all samples and indicating major separation between hippocampal and preoptic region (POA) structures (70%). POA samples: WT (n = 4) Ts65Dn (n = 4), Ts65Dn with miR200 overexpression (n = 4). Hippocampal samples: WT (n = 4) Ts65Dn (n = 3), Ts65Dn with miR200 overexpression (n = 4). (**B**) Pie chart refers to the number of genes upregulated and downregulated when comparing trisomic and wildtype littermates in the preoptic region (POA) (p_{adj} <0.05). Note that miR200b overexpression in the POA of Ts65Dn mice normalized the expression of all dysregulated preoptic genes, but *Gas5*. Interestingly, it has previously been shown that *Actr3* is down regulated in fetal DS brains (*134*) that cells expressing *Ly6a,* which is dysregulated in AD mice (*135*), can be regulated by GnRH *(136)*. **(C)** Protein network representation (STRING) of the down-regulated genes in Ts65Dn vs WT mice hippocampus. **(D)** UpSet plot showing intersection between differentially down-regulated genes in the hippocampus of Ts65Dn mice and genes rescued by miR200b in the hippocampus of Ts65Dn mice. **(E)** Representation of the genes found up-regulated in Ts65Dn mice and rescued by miR200b, showing strong association with myelination, oligodendrocyte differentiation and potassium ion transport. **(F)** Representative Western blot (top) and quantification (bottom) of Kir7.1 and Mbp protein expression in the hippocampus. Kir7.1: WT *vs*. Ts65Dn+miR200, $t_{(15)}$=6.58 *P*<0.001; Ts65Dn *vs*. Ts65Dn+miR200, $t_{(15)}$=6.05 *P*<0.001 ; n=6 per group. Mbp: WT *vs*. Ts65Dn, $t_{(14)}$=2.07 *P*<0.05; Ts65Dn *vs*. Ts65Dn+miR200, $t_{(14)}$=2.6 *P*<0.021 ; n=5 and 6. (**G**) RNA-seq data showing increased expression of Qk in the hippocampus of Ts65Dn mice (RNA-seq p-values ***P<0.0001). (Data are represented as mean ± SEM. For statistical analysis, *P* values were calculated by one-way ANOVA followed Tukey's multiple comparison post hoc test).

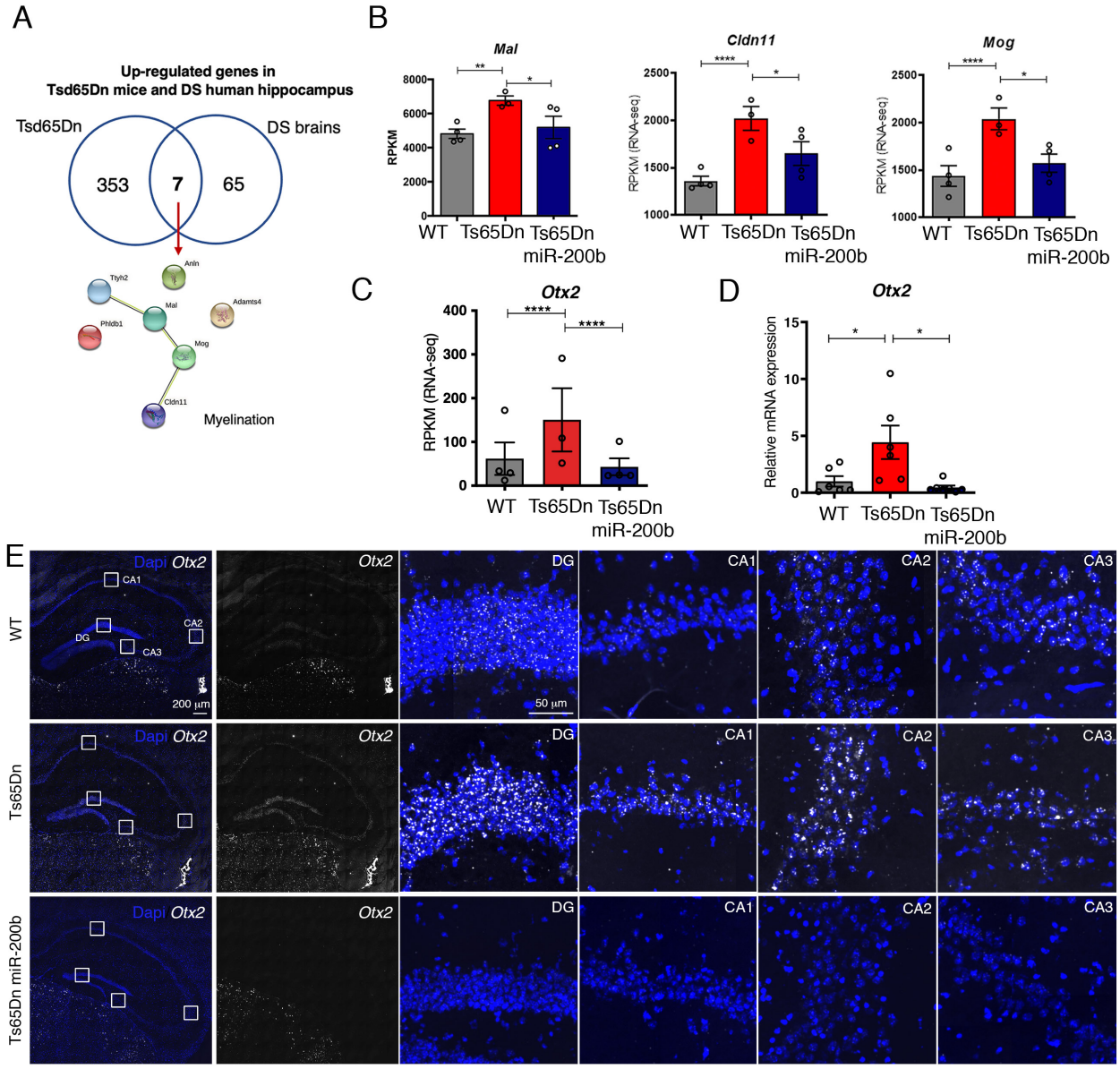

Fig. S12. Transcriptional alterations in myelination-related genes in Ts65Dn mice and DS human brains. (**A**) Venn diagram showing 7 common up-regulated genes between Ts65Dn hippocampus and DS human brains (hippocampus) (*35*) that are mostly related to myelination processes (*Mal, Mog, Cldn11*). (**B**) RNA-seq data of Ts65Dn mice hippocampus of myelination-associated genes. (RNA-seq p-values *$P < 0.01$; ** $P < 0.001$ **** $P < 0.00001$). (**C-E**) RNA-seq data (**C**), RT-qPCR (**D**) and fluorescent in situ hybridization assessment (**E**) of *Otx2* expression in the hippocampus of WT and Ts65Dn mice in the presence or absence of miR-200b overexpression in the preoptic region. Values represent means ± SEM. Statistical differences were tested using one way ANOVA and Tukey's posthoc test. ***$P<0.001$; *$P<0.05$. DG: dentate gyrus. (**F**) Venn diagram of the up-regulated genes found in TsDn65 mice hippocampus and in 10-month-old APP mice, in the CA1 region (*63*); 25 genes were found up-regulated in both datasets. Protein network analysis (STRING) showing that common up-regulated genes are mostly associated with axon ensheathment and oligodendrocyte/ myelination-related terms.

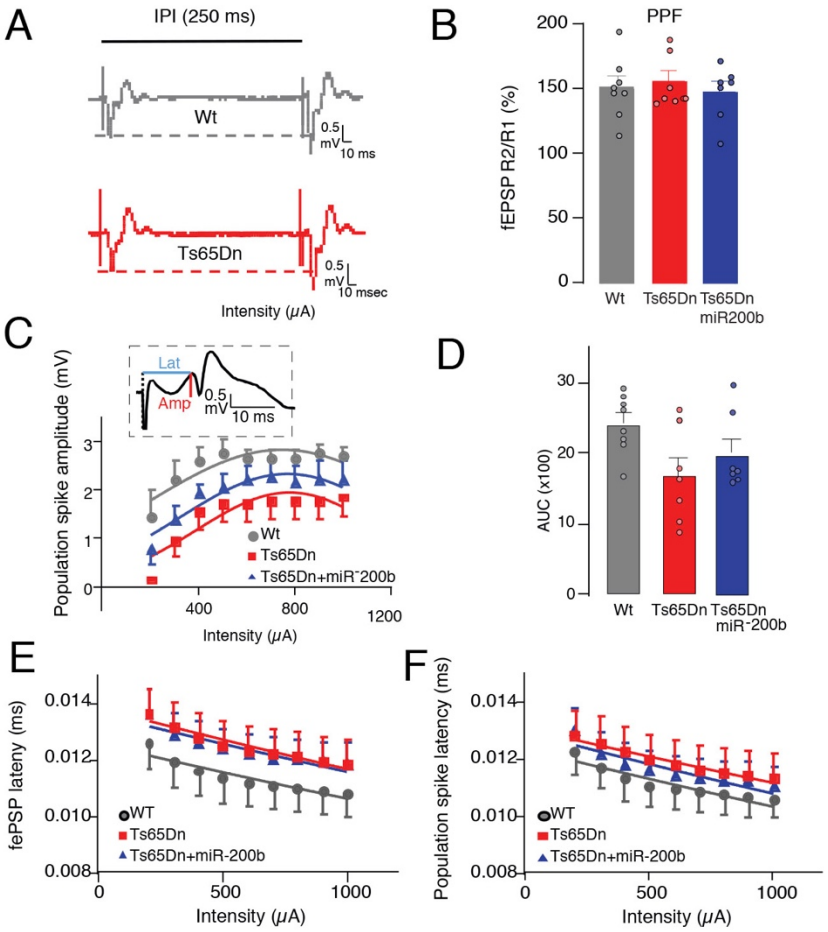

Figure S13. Impairment of the delay of the EPSP-population spike responses in the hippocampus *in vivo*. (**A**) Example traces show the fEPSP response to paired-pulse facilitation (PPF) stimulation at an interpulse interval (IPI) of 250 milliseconds (ms) in WT and Ts65Dn mice (scale: 0.5 mV, 10 ms). (**B**) The facilitation ratio values were computed as the ratio of the second stimulus-evoked fEPSP peak divided by the first stimulus-evoked fEPSP peak. The facilitation ratios of WT (gray bar), Ts65Dn (red bar) and Ts65Dn-miR200b (blue bar) mice were calculated from the averaged facilitation ratio values. The normalized facilitation ratio (R2/R1) indicated that there was no difference in PPF between all groups of mice, suggesting normal short-term plasticity. Data were given as mean (±SEM) and statistical differences were tested using a one-way repeated measure ANOVA (**B**: $F_{(2,19)} = 0.2343$, $P = 0.7934$). (**C**) Insert: schematic of a population spike recording with the measure of latency (horizontal blue bar) and of amplitude (vertical red bar) of the population spike. Similarly, the response of the population spike amplitude to commissural path stimulation at increasing stimulus intensities (population spike evoked by 200-1000 μA) showed a significant difference between groups of mice (**C**: Kurskall Wallis ANOVA; $F(26, 198) = 77.01$; $P < 0.0001$) and difference was significant for values of 400, 500, 700, 8000 and 900 μA ($P < 0.05$ using Mann-Whitney U test WT vs. Ts65Dn mice). (**D**) Area under the curve (AUC) of the population spike-induced responses was measured in WT (gray bar), Ts65Dn (red bar) and Ts65Dn-miR200b (blue bar) mice. Data are means ± SEM of AUC and one-way ANOVA showed a trend of decrease in Ts65Dn mice, suggesting a trend of lower somatic excitability of in Tg65Dn (**D**: $F(2, 19) = 3.4625$; $P = 0.0523$). (**E**) The latency of fEPSP response to commissural path stimulation at increasing stimulus intensities (fEPSP evoked by 200-1000 μA) showed no difference between groups of mice (**A**: Kruskall Wallis ANOVA; $F_{(26,198)} = 25.38$ $P > 0.497$). (**F**) Similarly, the delay of population spike response to commissural path stimulation at increasing stimulus intensities (fEPSP evoked by 200-1000 μA) showed no difference between groups of mice (**F**: Kruskall Wallis ANOVA; $F_{(26,198)} = 22.78$; $P > 0.645$).

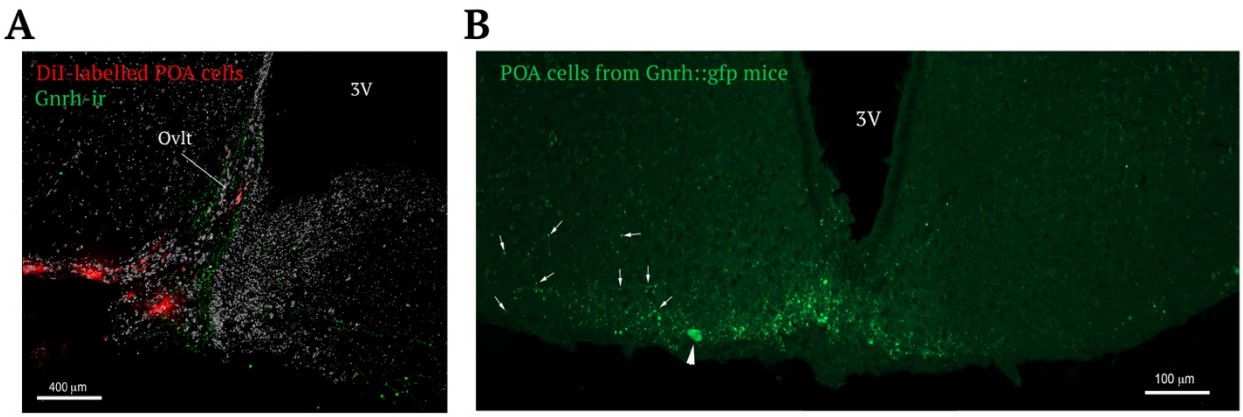

Fig. S14. Visualization of grafted POA cells in the brain of Ts65Dn mice. (**A**) Visualization of DiI-labelled cells in the region of the organum vasculosum laminae terminalis (Ovlt) after their infusion as a single cell suspension into the third ventricle (3V) in a sagittal section of Ts65Dn mouse preoptic region. Scale bar: 400 μm. (**B**) Localization of a GnRH neuron and GnRH fibres expressing GFP in a frontal section of the caudal tuberal region of the hypothalamus in a Ts65Dn mouse in which a suspension of cells dissociated from the POA of *Gnrh::gfp* P0 mice was grafted into the 3V. Scale bar: 100 μm.

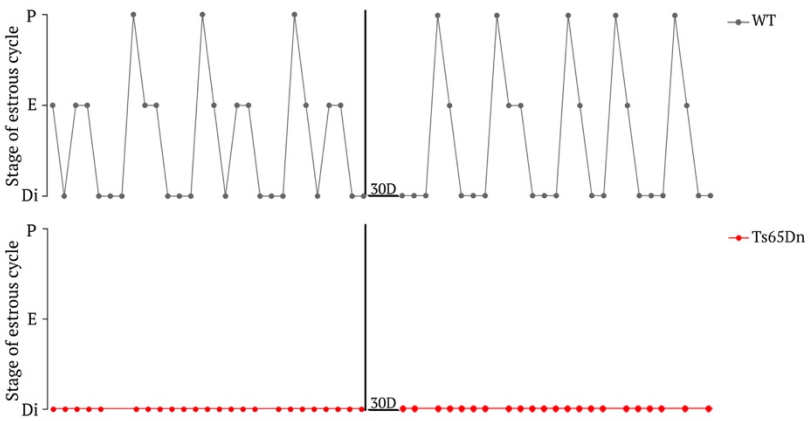

Fig. S15. Effect of brain surgery and cell grafting on oestrous cyclicity. Representative oestrous cyclicity of middle-aged (P360) WT and Ts65Dn female mice before and after brain surgery or the implantation of neonatal brain tissue containing WT GnRH neurons (WT-POA).

5

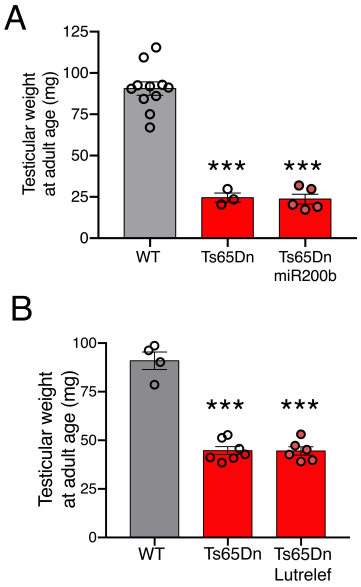

Fig. S16. Effect of 2-week miR-200b overexpression in the preoptic region (A) and pulsatile Lutrelef treatment (B) on testicular weight in Ts65Dn mice. Values represent means ± SEM. Statistical differences were tested using one-way ANOVA and Tukey's posthoc test. ***P<0.001.

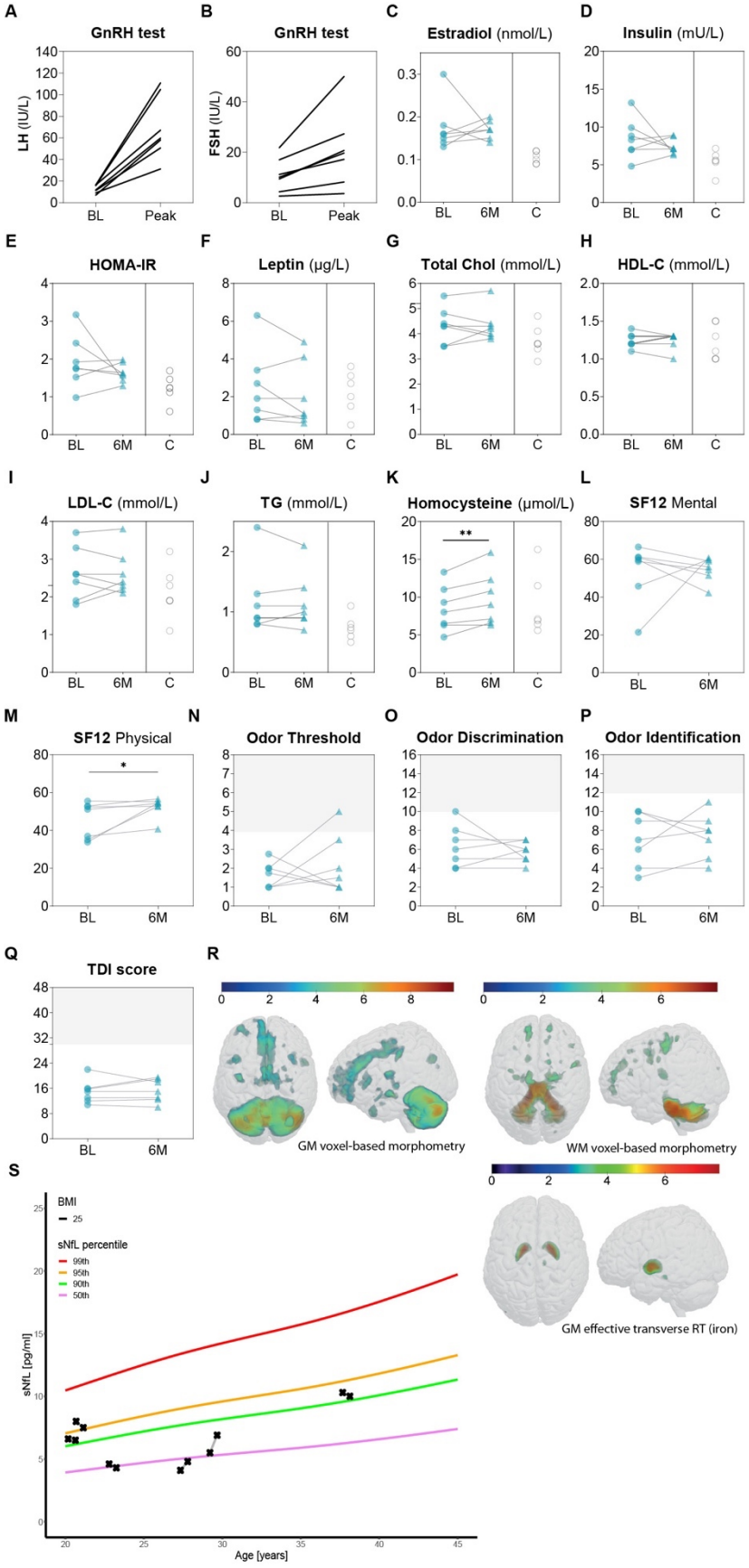
A
GnRH test
LH (IU/L)
BL
Peak
B
GnRH test
FSH (IU/L)
BL
Peak
C
Estradiol (nmol/L)
BL
6M
C
D
Insulin (mU/L)
BL
6M
C
E
HOMA-IR
BL
6M
C
F
Leptin (µg/L)
BL
6M
C
G
Total Chol (mmol/L)
BL
6M
C
H
HDL-C (mmol/L)
BL
6M
C
I
LDL-C (mmol/L)
BL
6M
C
J
TG (mmol/L)
BL
6M
C
K
Homocysteine (µmol/L)
**
BL
6M
C
L
SF12 Mental
BL
6M
M
SF12 Physical
*
BL
6M
N
Odor Threshold
BL
6M
O
Odor Discrimination
BL
6M
P
Odor Identification
BL
6M
Q
TDI score
BL
6M
R
GM voxel-based morphometry
WM voxel-based morphometry
S
BMI
25
sNfL percentile
99th
95th
90th
50th
sNfL [pg/ml]
Age [years]
GM effective transverse RT (iron)

Fig. S17. **Clinical data at baseline and after 6-month of pulsatile GnRH therapy in DS subjects.** (**A-B**) **GnRH test** (100 μg iv of LHRH): baseline (BL) to peak differences in LH and FSH. (**C-K**) Biochemical parameters at BL (blue dots) and after 6 months (6M) of GnRH therapy (blue triangles) compared to healthy controls (open circles). (**L-M**) **Quality of life**, evaluated by 12-Item Short Form Survey (SF-12): (**L**) Physical composite score (45.4±3.6 vs 52.4±2.0, *P*=0.075); (**M**) mental composite score (53.4±5.9 vs 54.79±2.4, *P*=0.859). (**N-Q**) **Olfaction** using the Sniffin' Sticks tests: (**N**) threshold score (1.6±0.3 vs 2.1±0.2, *P*= 0.489); (**O**) discrimination score (6.3±0.8 vs 5.7±0.2, *P*=0.535); (**P**) identification score (7.0±1.1 vs 7.4±0.3, *P*=0.682); (**Q**) TDI score (global olfactory scores: 14.9±1.4 vs 15.3±0.5, *P*=0.723). (**R**) **Magnetic resonance imaging**: MT (magnetization transfer); RT (relaxation rate). Voxel-based quantification of the effective transverse relaxation rate R2* indicative for iron content revealed increased iron content in pallidum bilaterally and a trend in the substantia nigra for patients with DS. (**S**) **Serum neurofilament light chain** (sNfL) levels (black cross) compared to healthy controls' sNfL Z-scores (reference database includes 4532 samples, (*44*)).

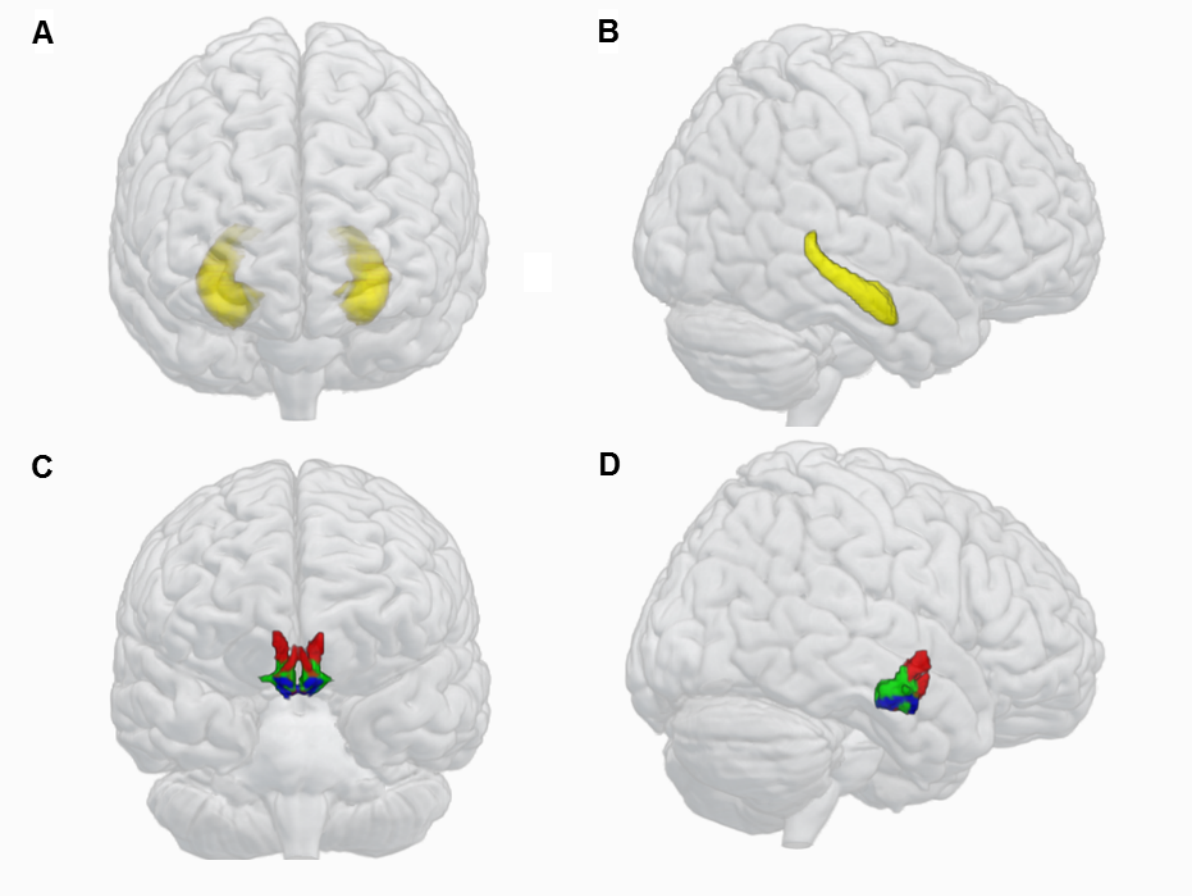

Fig. S18. 3D reconstruction of specific cerebral regions of interest on the brain map template. (**A-B**) Hippocampi: coronal (**A**) and sagittal (**B**) views. (**C-D**) Hypothalamic nuclei: coronal (**C**) and sagittal (**D**) views. Longitudinal analyses' results on DS subjects who received 6-month GnRH treatment can be found in **Table S6**. *Yellow: hippocampi; red: anterior hypothalamic nuclei; green: lateral hypothalamic nuclei; blue: posterior hypothalamic nuclei*.

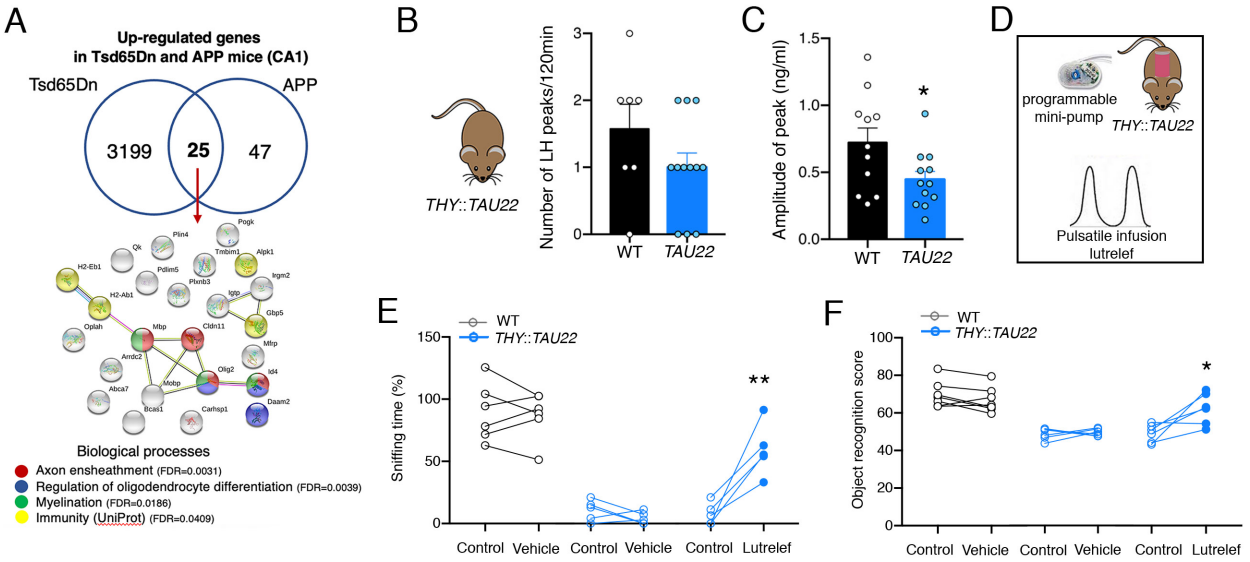

Fig. S19. Transcriptional alterations in myelination-related genes in Ts65Dn mice and a mouse model of Alzheimer disease (AD) and the rescue of olfactory and cognitive impairments by pulsatile Lutrelef in *THY*::*TAU22* mice. (**A**) Venn diagram of the up-regulated genes found in TsDn65 mice hippocampus and in 10-month-old APP mice, in the CA1 region (*63*); 25 genes were found up-regulated in both datasets. Protein network analysis (STRING) showing that common up-regulated genes are mostly associated with axon ensheathment and oligodendrocyte/ myelination-related terms. (**B-F**) Assessment of pulsatile LH release by serial blood sampling in THY::TAU22 mice showed that they had a normal LH pulse frequency (**B**), but a significantly decreased LH pulse amplitude (**C**) compared to WT littermates. Values represent means ± SEM. Statistical differences were tested using an unpaired Student's t-test or a Mann-Whitney U test. (**B**: WT vs. *THY*::*TAU22*, $t(17) = 1.44$, $P = 0.17$, $n = 7$ and 12. **C**: WT vs. *THY*::*TAU22*, $t(21) = 2.26$, $P = 0.03$, $n = 11$ and 12). * $P < 0.05$. (**D-F**) Lutrelef pulsatile infusion (**D**) rescued the capacity to discriminate between different odors (**E**) and objects (**F**) in *THY*::*TAU22*mice. Every dot represents one subject. Statistical differences were tested using a paired Student's t-test or a Wilcoxon matched-pair test. (**E**: WT control vs. WT infusion vehicle, $t(5) = 0.38$, $P = 0.72$, $n = 6$; *THY*::*TAU22* control vs. *THY*::*TAU22* infusion vehicle, $t(5) = 0.46$, $P = 0.67$, $n = 6$; THY::TAU22 control vs. *THY*::*TAU22* pulsatile infusion Lutrelef, $t(4) = 4.72$, $P = 0.009$, $n = 5$. **F**: WT control vs. WT infusion vehicle, $t(6) = 1.84$, $P = 0.11$, $n = 7$; *THY*::*TAU22* control vs. *THY*::*TAU22* infusion vehicle, $t(5) = 0.46$, $P = 0.67$, $n = 6$; *THY*::*TAU22* control vs. *THY*::*TAU22* pulsatile infusion Lutrelef, $t(5) = 3.09$, $P = 0.03$, $n = 6$).** $P < 0.01$; *** $P < 0.001$.

Table S1 – Clinical and biochemical features at baseline and after 6 months of GnRH therapy

	Down syndrome (DS), n=7			Healthy controls, n=6	
	BL	**6M**	***P-value*** BL vs 6M	**Controls**	***P-value*** BL vs controls
Clinical parameters					
Age (years)	26.4 ± 2.3	-	-	25.1 ± 2.0	0.690
Body mass index (kg/m²)	22.8 ± 1.0	22.8 ± 1.2	0.999	22.7 ± 0.5	0.893
Testicular volume Prader orchidometer (mL)	15.7 ± 1.0	16.4 ± 1.1	0.356	-	-
Reproductive profile					
Total testosterone (nmol/L)	24.8 ± 2.9	25.6 ± 2.3	0.763	23.4 ± 2.1	0.702
Estradiol (nmol/L)	0.17 ± 0.02	0.17 ± 0.01	0.703	0.11 ± 0.01	**0.0012**
LH (IU/L)	12.4 ± 1.4	12.3 ± 1.3	0.935	3.4 ± 0.6	**0.0002**
FSH (IU/L)	10.9 ± 2.5	7.2 ± 1.6	**0.018**	2.4 ± 0.7	**0.012**
Inhibin B (pg/mL)	143.1 ± 28.8	137.6 ± 25.5	0.590	206.8 ± 15.0	0.114
Metabolic profile					
Glucose (mmol/L)	5.1 ± 0.2	5.0 ± 0.1	0.253	5.0 ± 0.1	0.731
Insulin (mU/L)	8.4 ± 1.0	7.4 ± 0.4	0.405	5.4 ± 0.6	**0.032**
HOMA-IR	1.9 ± 0.3	1.6 ± 0.1	0.338	1.2 ± 0.1	**0.034**
hsCRP (mg/L)	5.0 ± 1.6	3.7 ± 1.3	0.344	0.3 ± 0.1	**0.008**
Leptin (μg/L)	2.5 ± 0.7	2.1 ± 0.7	0.344	2.2 ± 0.6	0.810
Total cholesterol (mmol/L)	4.3 ± 0.3	4.3 ± 0.2	0.813	3.7 ± 0.3	0.127
Triglycerides (mmol/L)	1.0 ± 0.1	1.0 ± 0.1	0.999	0.7 ± 0.1	0.026
HDL-cholesterol (mmol/L)	1.2 ± 0.04	1.2 ± 0.04	0.999	1.2 ± 0.1	0.923
LDL-cholesterol (mmol/L)	2.6 ± 0.3	2.6 ± 0.2	0.915	2.2 ± 0.3	0.256
ALAT (IU/L)	43.9 ± 10.5	34.7 ± 8.0	0.297	19.0 ± 2.0	0.055
ASAT (IU/L)	28.3 ± 4.0	23.0 ± 3.8	0.092	22.7 ± 2.3	0.265
Total homocysteine (μmol/L)	8.4 ± 1.1	9.7 ± 1.3	**0.008**	9.0 ± 1.7	0.796

Baseline (BL), 6 months (6M), Values are expressed as means ± SEM. For inhibin-B in controls, n=5.

5

Table S2. Structural MRI results in DS patients vs controls (as shown in Figure 7N).

Tissue class	Contrast	MRI feature	Region	Side	peak voxel-level			coordinates (mm)		
					pFWE-corr	T	Z	x	y	z
GREY MATTER	**CTR > DS**	**volume (VBM)**	*cerebellum*	L	<0.0001	9.89	7.3	-14	-50	-51
				R	<0.0001	8.68	6.72	44	-69	-27
			anterior cingulate cortex	R	0.001	6.42	5.44	2	33	27
			supplementary motor cortex	R	0.006	5.81	5.04	3	-9	50
			substantia nigra	L	0.002	6.22	5.31	-8	-18	-15
				R	0.006	5.84	5.07	12	-14	-15
			thalamus	R	0.003	6	5.17	2	-12	17
			insula	L	0.028	5.31	4.7	-48	12	-9
				R	0.004	5.97	5.15	54	12	-6
			M1	L	0.004	5.96	5.15	-35	-21	45
	CTR < DS		*middle temporal gyrus*	L	0.045	5.16	4.59	-59	-33	-32
				R	0.034	5.25	4.66	62	-15	-17
			adjacent to							

WHITE MATTER	**CTR > DS**	**volume (VBM)**	*cerebellum*	L	<0.0001	7.96	6.35	-14	-35	-30
				R	<0.0001	7.83	6.28	24	-51	-32
			M1	L	0.055*	4.95	4.44	-12	-15	50
				R	0.017	5.35	4.86	18	-17	57
			superior frontal gyrus	L	0.095*	4.76	4.29	-15	42	32
				R	0.65*	3.89	3.61	15	51	15
			middle temporal gyrus	L	0.029	5.17	4.6	-33	-50	-8
				R	0.002	6.11	5.24	45	-27	-23
GREY MATTER	**CTR > DS**	**MT saturation (myelin)**	*thalamus*	L	<0.0001	7.62	6.18	-23	-33	8
				R	<0.0001	7.41	6.06	15	14	18
			M1	L	<0.0001	6.9	5.76	-2	-18	53
				R	<0.0001	6.78	5.69	6	-23	54
			S1	L	0.032	5.36	4.74	-63	-20	29
				R	0.004	6.27	5.36	65	-15	21
			angular gyrus	L	0.002	6.29	5.37	-63	-57	24
				R	0.005	5.93	5.14	59	-60	26

			insula	L	0.029	5.38	4.76	-47	8	2
				R	0.06*	5.01	4.38	57	18	6
			adjacent to							
WHITE MATTER	**CTR > DS**	**MT saturation (myelin)**	*M1*	L	<0.0001	7.3	6	-15	-18	71
				R	<0.0001	7.07	5.86	21	-20	69
			S1	L	0.004	5.35	4.75	-14	-33	71
				R	<0.0001	9.76	7.27	5	-30	66
			superior frontal gyrus	L	<0.0001	6	5.2	-9	60	6
				R	<0.0001	6.28	5.32	9	60	2
			superior temporal gyrus	L	0.002	5.53	4.86	-63	-29	6
				R	<0.0001	6.8	5.65	63	-15	5
GREY MATTER	**CTR < DS**	**effective transverse relaxation R2* (iron)**	pallidum	L	<0.0001	7.6	6.17	-14	2	2
				R	<0.0001	7.99	6.38	23	-9	2
			substantia nigra	L	0.86*	3.79	3.54	-11	-20	-14
				R	0.37*	4.35	3.99	12	-18	-14

Table S3 – Structural MRI longitudinal analysis (baseline vs 6-month GnRH therapy in DS subjects) after small volume correction with hypothalamus & hippocampus masks.

Tissue class	Contrast	MRI feature	Region	Side	peak voxel-level			coordinates (mm)		
					pFWE-corr	T	Z	x	y	z
GREY MATTER	Positive correlation delta MoCA	volume (VBM)	*anterior hypothalamus*		0.5*	2.22	1.78	3	-2	-9
			lateral hypothalamus		0.4*	2.41	1.88	3	-3	-11
			hippocampus	R	0.47*	4.19	2.63	20	-11	-26
			hippocampus	L	0.75*	2.92	2.14	-35	-18	-18
	Positive correlation delta MoCA	MT saturation (myelin)	*hippocampus*	R	0.92*	2.12	1.72	29	-6	-29
			hippocampus	L	0.93*	2.02	1.66	-30	-9	-21
	Positive correlation delta MoCA	effective transverse relaxation R2* (iron)	*hippocampus*	R	0.9*	2.7	2.03	32	-35	-3
			hippocampus	L	0.77*	3.48	2.37	-24	-38	3

*Trends not surviving the threshold of $p_{FWE}<0.05$ correction for multiple comparisons

Table S4. Primers used for genotyping

Primer	Sequence 5' → 3'	Genotype
65Dn-F	GTG GCA AGA GAC TCA AAT TCA AC	Ts65Dn
65Dn-R	TGG CTT ATT ATT ATC AGG GCA TTT	
OIMR7338	CTA GGC CAC AGA ATT GAA AGA TCT	
OIMR7339	GTA GGT GGA AAT TCT AGC ATC C	
GnRHCre-F	CTG GTG TAG CTG ATG ATC CG	*Gnrh::Cre*
GnRHCre-R	ATG GCT AAT CGC CAT CTT CC	
GnRHGFP-F1	GAA GTA CTC AAC CTA CCA ACG GAA G	*Gnrh::Gfp*
GnRHGFP-R1	GCC ATC CAG TTC CAC GAG AAT TGG	
Tox-F	CGT GTT CCA CTC GAA GAG TT	iBot
Tox-R	GGC AAA ACT TCA TTT GCA TT	
TAU 23	CGC CCC GTG GTC TGT CTT GGC	TAU22
TAU 25	CCA ACC CCA CCC ACC CGG GAG	
Dicer-F1	CCT GAC AGT GAC GGT CCA AAG	$Dicer^{loxP/loxP}$
Dicer-R1	CAT GAC TCT TCA ACT CAA ACT	

Table S5. Antibodies used for western blot analysis

Primary antibody	Animal	saturation	Secondary antibody
APPCter-C17 (1/10000)	Rabbit, polyclonal	Milk 5%	Rabbit (*137*)
TauCter 994 S4 (1/10 000)	Rabbit, polyclonal	Milk 5%	Rabbit (*138*)
GAPDH (1/50000) (Sigma, RRID:AB_796208)	Rabbit, polyclonal	Milk 5%	Rabbit (Vector)
RelA, pRelA (1/500) (Cell Signaling, #8214, RRID:AB_1658204)	Rabbit, polyclonal	BSA 5%	Rabbit (*138*)
Anti-Kir7.1 (1/500) (Alomone labs, #APC-125, RRID:AB_10560908)	Rabbit, polyclonal	BSA 5%	Rabbit
MBP (1/1000) (Abcam, #ab40390, RRID:AB_1141521)	Rabbit, polyclonal	BSA 5%	Rabbit

Table S6. Primers used for real-time PCR

Gene	TaqMan® Gene Expression Assays
Actb	Actb-Mm00607939_s1
Cebpb	Cebpb-Mm00843434_s1
Dicer1	Dicer1-Mm00521722_m1
Gnrh1	Gnrh1-Mm01315605_m1
Kiss1	*Kiss1*-Mm03058560_m1
Kiss1-r	*Kiss1r*-Mm00475046_m1
Nos1	*Nos1*-Mm01208059_m1
Nf-κB1	*Nfkb1*-Mm004763361_m1
Otx2	Otx2-Mm00446859_m1
Meis1	Meis1-Mm00487664_m1
sGC	Gucy1b3-Mm00516926_m1
Zeb1	Zeb1-Mm00495564_m1
Primers ID	Maxima First Strand cDNA Synthesis Kit (Thermo Scientific)
mmu_RTqPCR_Kcnj13-F	CCACAAAGGAACCGAGAAACA
mmu_RTqPCR_Kcnj13-R	CCATCCATCTGAAGTGTGCT
mmu_RTqPCR_Aqp1-F	GATTGACTACACTGGCTGCG
mmu_RTqPCR_Aqp1-R	CACCCAGAAAATCCAGTGGT
mmu_RTqPCR_Id4-F	GCTCAACACTGACCCGG
mmu_RTqPCR_Id4-R	TCTTAATTTCTGCTCTGGCCC

miRNA	TaqMan® Gene Expression Assays
miR-141	mmu-miR-141-00463
miR-200a	mmu-miR-200a-000502
miR-200b	mmu-miR-200b-002251
miR-200c	mmu-miR-200c-002300
miR-429	mmu-miR-429-001077
miR-155	mmu-miR-155-002571
miR-125b	hsa-miR-125b-000449
miR-802	mmu-miR-802-002029
miR-99a	hsa-miR-99a-000435
let-7c	hsa-let-7c-0003799

Other Supplementary Materials for this manuscript include the following.

Table S7.

Additional statistical analyses by figure panel not listed in the legends.

Movie S1.

3D visualization of GnRH immunoreactivity in the brain of a P90 WT mouse.

Movie S2.

Optical reslice of a P90 WT mouse transparent brain showing GnRH immunoreactivity.